2018

Flexural Analysis of 3D Printed Members

Yazen Hindieh

FLEXURAL ANALYSIS OF 3D PRINTED MEMBERS

BY

YAZEN HINDIEH

A thesis submitted in partial fulfillment of the requirements for the

Master of Science

Major in Civil Engineering

South Dakota State University

2018

FLEXURAL ANALYSIS OF 3D PRINTED MEMBERS

YAZEN HINDIEH

This thesis is approved as a creditable and independent investigation by a candidate for Master's in Civil Engineering degree and is acceptable for meeting the thesis requirements for this degree. Acceptance of this does not imply that the conclusions reached by the candidate are necessarily the conclusion of the major department.

Suzette Burckhard
Advisor, Civil and Environmental Engineering Department Date

Nadim Wehbe
Head, Civil and Environmental Engineering Department Date

Dean, Graduate School Date

ACKNOWLEDGEMENT

I would like to acknowledge the NSF 1642037, OLC, SDSU and SDSMT Pre-Engineering Education Collaborative-II (OSSPEEC-II) for supporting and funding this research. I am indebted to Dr. Suzette Burckhard, OSSPEEC interns at SDSU; Calvin Wampol and Salvador Caballero; and Dr. Todd Letcher for their technical support and help with my research.

Additionally, I would like to thank all the Civil Engineering professors and instructors for providing me with the knowledge I have gained in Civil Engineering

TABLE OF CONTENT

ABBREVIATIONS

CT Beam = Cap on Top Beam

CB Beam = Cap on Bottom Beam

NC Beam = Beam with a filling hole beam and No Cap

M = the bending moment

P = the applied load

L = the span length between the two supports

σ_f = is the flexural stress

d= is the depth of the beam in the z-direction

I= is the moment of inertia of the beam

ε_f = Flexural strain.

D= deflection at the center of the beam.

s = the standard deviation

x = value of a single observation

X = mean value of the set of observations

n = number of observations

LIST OF FIGURES

LIST OF TABLES

ABSTRACT

FLEXURAL ANALYSIS 3D PRINTED MEMBERS

YAZEN HINDIEH

2018

Flexural analysis of a beam is the determination of the bending capacity of the beam when it is undergoing a load causing the beam to bend. 3D printed plastic beams have not been characterized and analyzed yet. However, this research characterizes 3D-printed PLA beams and provides projects for future researchers. The literature describes several fields that utilizes 3D-printing. In this research, we introduce an innovative approach to investigate the flexural properties of a 3D printed composite beam, made of PLA and locally available soil. The flexural testing will determine the behavior and mechanical properties of the 3D printed beams. The flexural properties of the beams were analyzed by following ASTM D790*, Standard Test Methods for Flexural Properties of Unreinforced and Reinforced Plastic and Electrical Insulation Material*. Then design enhancements were done to improve the beams' flexural capacity and overall strength. In this research, it was discovered that incorporating sand in the beam reduces the flexural capacity of the beams. Also, that the flexural behavior of the PLA beams is similar to non-reinforced timber beams.

Introduction

The objective of this research is to provide projects for Oglala Lakota College (OLD) students, and design and characterize 3D printed beams. A broader impact of this research is to help protect the environment by utilizing non-biodegradable materials in landfills and maybe a start to researching the usage of 3D printed plastic beams in structures. In addition, to making it more feasible for people in the poorer neighborhoods to afford better housing. PLA is a cost-effective product that allows for a more affordable building material needing less workers and cheaper materials. According to a statistical study by Paul Jargowsky, 13.8 million families in “the bigger” cities of the United States only live in high-poverty neighborhoods. Most people living in high poverty neighborhoods have lower incomes and as a consequence live in poor conditions. Poor housing is a problem in the U.S., however many of these lower income families cannot afford better homes. Also, an average American 185 pound of plastic waste a year, and that creates an environmental problem since only 10% of that is recycled (Semuels, 2015). To try and help find a solution to these two problems, this research utilizes a thermoplastic, polylactic acid (PLA), and locally-available soil to build structural beams. These beams will be used as the model system to investigate flexural strength and deformation of the 3D printed members. Flexural strength will be tested to determine the behavior and mechanical properties of the composite beams. The beams consisted of 3D printed PLA hollow boxes and fine-grain soil, more specifically Unimin sand. The samples will then be to tested for flexural properties by following ASTM D790, *Standard Test Methods for Flexural Properties of Unreinforced and Reinforced Plastic and Electrical Insulation Material*. Five samples of each design were printed to ensure quality

control. The design followed a cyclic design method; first an initial design was completed and tested, second stage is to reduce the data to mechanical properties, and finally improve the design in relation to behavior of the tested beam.

From this research it was concluded that, the hollow beams without Unimin sand have higher flexural capacity than ones with Unimin sand.; since Unimin sand causes interlayer adhesion failure. Beams without Unimin sand behaved like timber beams; where they underwent a brittle flexural failure. Brittle failures are not preferred in engineering since it does not provide any warning time for the public. The usage of Fiber Reinforced Plastic (FRP) can be advantageous in regards to the interlayer adhesion failure and brittle failure.

Literature Review

2.1 History of 3D Printing

3D printing is a series of two-dimensional printing in layers used to build 3D object that is designed using computer-aided design programs, like SolidWorks and Auto-Cad. This paper will address the history of flexural analysis, and the usage of PLA and fine grain soil to create 3D printed beams.

3D printing was first designed and engineered in 1986 by Chuck Hull, it was known as Fused Deposition Modeling (FDM) (Gross, 2014).

> "3D printing is a process for making a component by depositing a first layer of a powder material in a confined region and then depositing a binder material to selected regions of the layer of powder material to produce a layer of bonded powder material at the selected regions. Such steps are repeated a selected number

> of times to produce successive layers of selected regions of bonded powder material so as to form the desired component" (Sachs, 1994)

Using Hull's 3D MIT professors Cima and Sachs patented the first machine termed "3D printer" in 1993 and it was developed to print plastic, metal and ceramic parts (Cima, 1994). 3D printed members are designed using a computer aided design (CAD) program, e.g., AutoCad, SolidWorks, AutoDesk and others (Gross, 2014). It was not until after 3D printers were available to the public that 3D printing truly advanced.

2.2 Applications of 3D Printing

First 3D printing started as a use for artists and designers to preview their design prior to production. 3D printing has vital advantages in terms of cost effectiveness, efficiency (less time), accuracy, and how it can be used in almost every field of work (Panda, 2017). According to Verntola's research, 3D printing was a breakthrough in the medical field. Robotic prosthetics were designed that are to fit the needs of the patients for only $300 (Ventola, 2014). This research show that these prosthetic robotic hands can be accurately sized, have an independent thumb movement, and weight less than most externally powered prostheses (Gretsch, 2015).

2.3 3D Printing in Civil Engineering

3D printing has been used in the geotechnical engineering field, and the structural engineering field. In the geotechnical field, natural and synthetic, 3D printed, fibers were studied for use as soil reinforcement. Fibers were 0.2-4% of the weight of the soil. The results showed an increase in strength and stiffness when using these fibers

due to their mechanical properties (Hejazi, 2012). In the structural field, 3D printing of concrete structures used large scale 3D printers and ultra-high-performance concrete, using an FDM like technique.

2.4 Beams

Beams are structural members that are normally horizontally oriented. Beams primarily withstands bending loads, that is why they are used to support roofs, and floor slabs. In engineering terminology bending loads are defined as flexural loads. Flexural loads are externally applied loads that cause beams to bend. Beams are made of many different materials like only steel, reinforced concrete, prestressed concrete, timber, and reinforced timber. Those materials are chosen based on efficiency, load carrying capacity, aesthetics, and most importantly feasibility (cost). Beams are designed and analyzed based on their flexural strength and capacity.

2.5 Polylactic Acid (PLA)

PLA is a plastic acquired in 1932 by Carothers. PLA is manufactured by fermentation and chemical synthesis (Lee, 2014). Plastics are non-biodegradable, for that their disposal is an environmental problem. Utilizing plastics as a building material would decrease the amount of plastic waste around the world. Currently, PLA is used in packaging and a many medical applications one of which is 3D printed casts (Dodziuk, 2016). The reason behind the versatile use of PLA is that it is a thermoplastic that is easily 3D printed, having properties similar to Polyethylene.

2.6 Three-Point Flexural Test.

Flexural strength can be defined as the resistance of a member to bending. Bending of a member using three-point flexure testing can be obtained by applying a point load at the center of the beam causing bending moments throughout member, with the highest bending moment at the center of the beam; as illustrated in Figure 3.3.1. Force-displacement data are usually obtained from the three-point flexural test. After that, the flexural properties of the member can be determined through a flexural stress-strain diagram which would lead to shear strength, flexural modulus and other important mechanical properties.

Stress-strain graphs include the stress values on the y-axis and the strain values on the x-axis. Flexural stress is controlled by the bending moment, moment of inertia and the distance to the neutral axis. Strain can be defined as the ratio of displacement to the original length. Flexural modulus is the ratio of stress to strain in the elastic region of the stress-strain graph. Figure 2.6.1 is added to display the important regions and vital points in a stress-strain diagram. Keep in mind, Figure 2.6.1 is an idealized tensile stress-strain diagram.

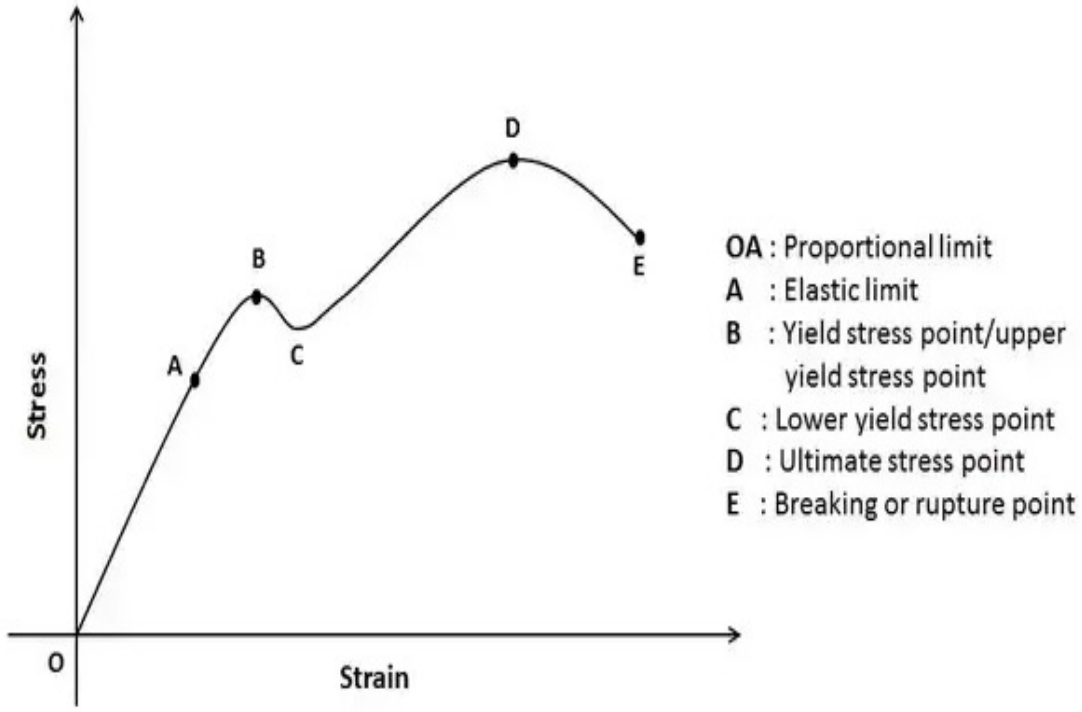

Figure 2.6.1. This figure displays the important regions and vital points in an idealized tensile-stress-strain diagram with defined engineering properties points provided. (Quora.com)

The points illustrated on Figure 2.6.1 represent the key points on a stress-strain diagram. Point A is the elastic limit (end of the elastic region), the slope of the straight line before point A can be used to identify the value of modulus of elasticity. Point B is the is the yield point, which a point where the sample tested goes from the elastic region into a plastic region. Point D is the ultimate stress and point E is the failure point. Failure point is defined differently among scholars, some scholar consider a failure when the stress capacity decreases by a certain percentage and some scholars consider rupture as the failure point.

Materials and Methods

The beams outer shell was made of PLA and the interior of the beams was packed Unimin sand. PLA was chosen since its properties make it an ideal thermoplastic to use with the present 3D printer's limitations of heat insulation and production. To 3D print PLA the nozzle should be at 190-200 ^{o}C. and the plate at 60 ^{o}C (Yao, 2017). Table 3.1 shows the PLA's mechanical properties

Table 3.1 Mechanical properties of PLA (Makeitfrom, 2015).

Elongation	6%
Flexural Modulus	4 GPa
Flexural Strength	80 MPa
Tensile strength	50 MPa

The reasoning behind adding a soil was to reduce the stress acting on the PLA by increasing the moment of inertia of the beam, given that the flexural stress, σ_f, and moment of inertia, I, are inversely proportional to one another (equation 3.1).

$$\sigma_f = \frac{Mc}{I} \qquad \text{Equation 3.1}$$

Additionally, the soil within the beam would help distribute the force "equally" along the beam, Figure 3.1.

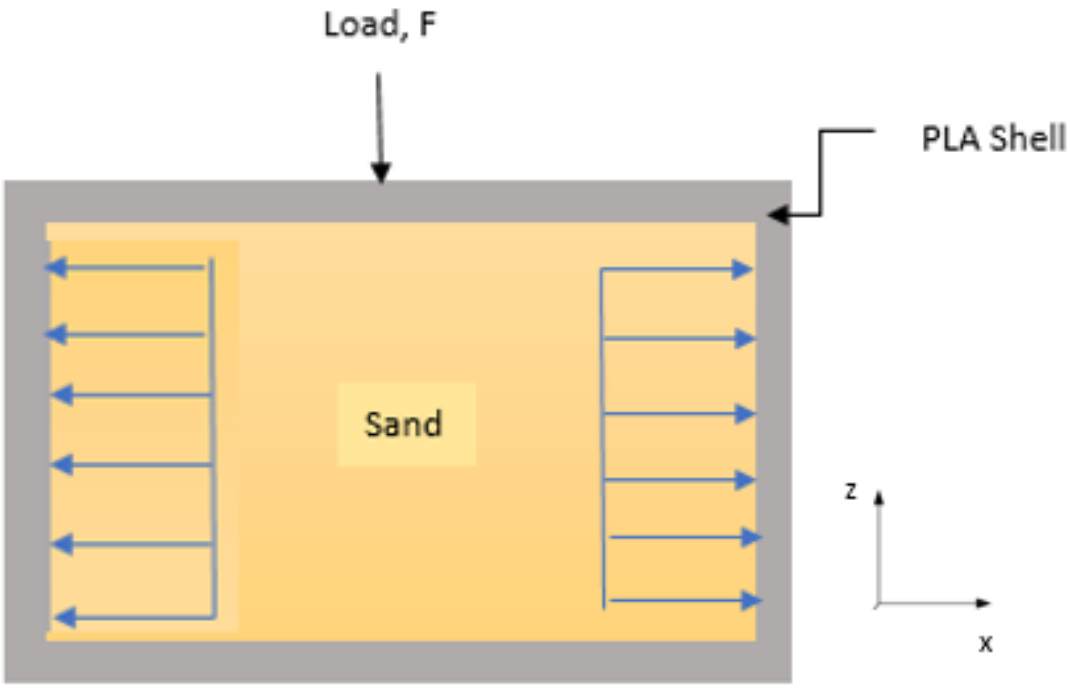

Figure 3.1. This figure (x-z axes) represents the sand changing the orientation of the point load (F) to a horizontal distributed load along all the walls (y-z axes too) of the box beam.

The soil used in this research was Unimin sand. Unimin sand is a cohesionless soil and have a uniform grain size (0.15 mm). The usage of different types of soil may affect the behavior of the composite beams. The following are the steps followed to perform the flexural analysis of the composite beams:

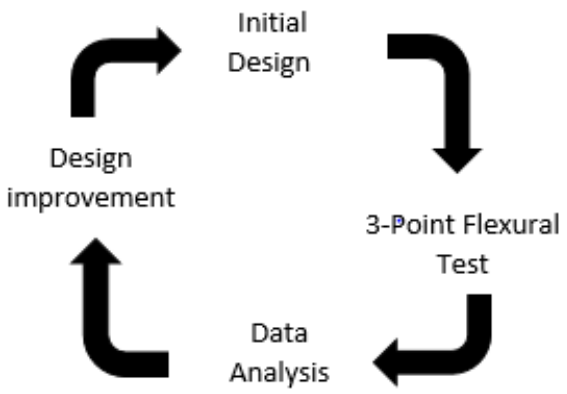

Figure 3.2. Design cycle.

3.1 Sample Identification

The research included three different beam designs and are identified in Table 3.1.1.

Table 3.1.1 Design samples abbreviations.

Design number and Name	Abbreviation
Design 1: Cap on Top	CT beam
Design 2: Cap on the Bottom	CB beam
Design 3: Beam with a filling hole and No Cap	NC beam

3.2 Initial Design

The initial design of the composite beam was a hollow box that is enclosing Unimin sand by a cap on top, top of the z-axis. The beams was assembled using Solidworks, Figure 3.2.1.

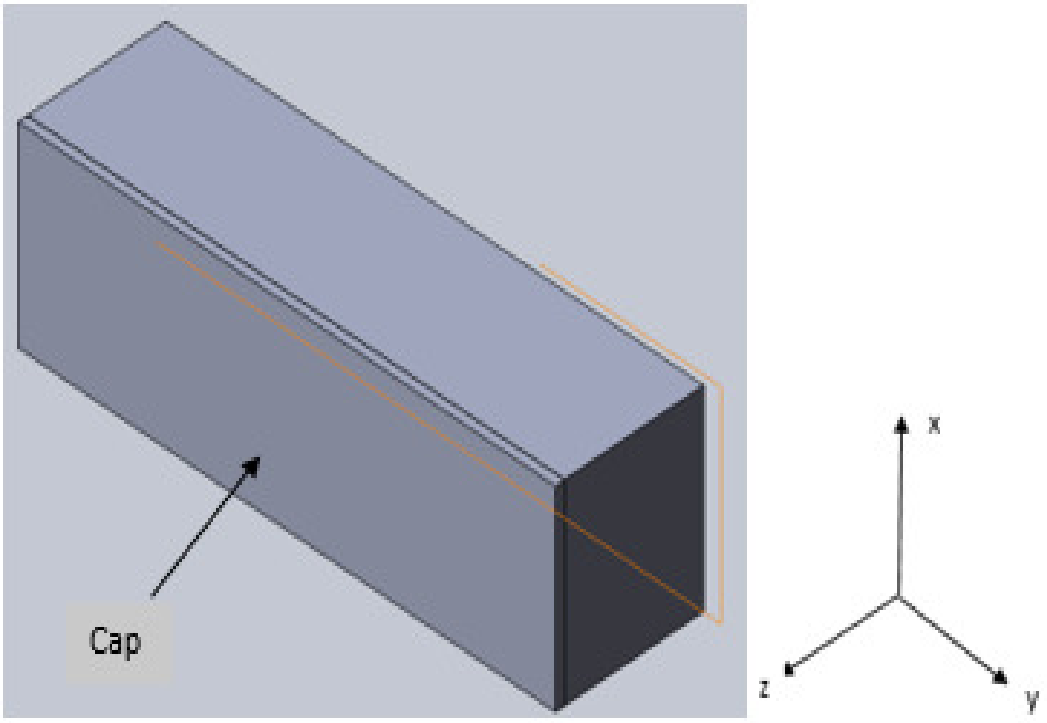

Figure 3.2.1. Assembled CT beam to show perfect cap-to-box fit.

The beam was designed in two parts on SolidWorks and then SolidWorks was used to assemble them together to ensure the dimensions of the two parts match with tolerance, first part was the box and the second part was the cap. They were designed to fit together with tolerance, refer to Figure 3.2.2 and 3.2.3 to see the two parts and how their dimensions fit with tolerance. The reason behind designing and printing the parts separately is to allow the sand to be placed inside the hollow box and packed correctly before the box was put together.

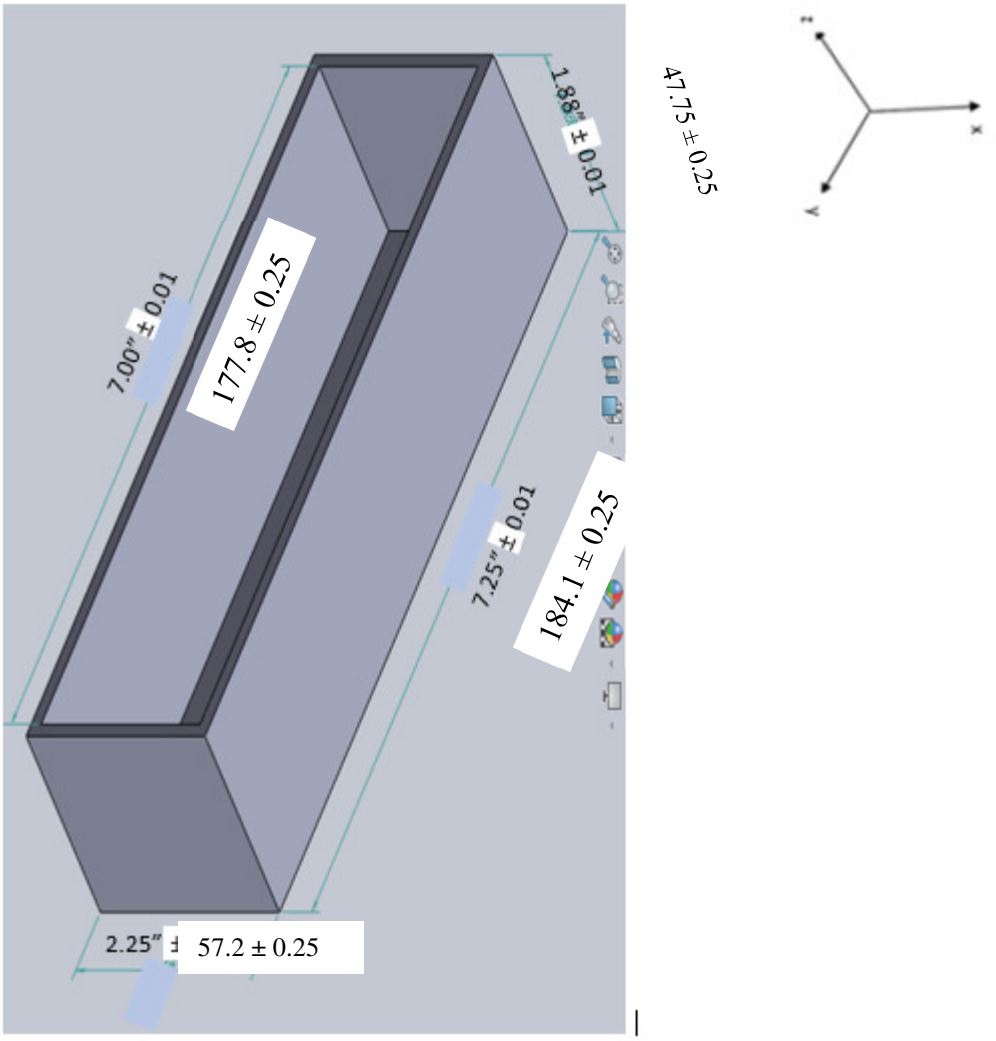

Figure 3.2.2. Dimensions of the boxes for both CT and CB beams (mm).

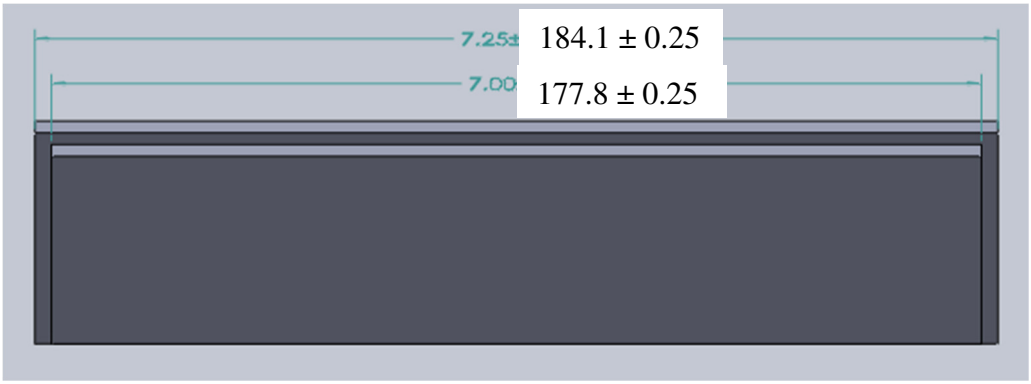

Figure 3.2.3. Dimensions of the cap for both CT and CB beams (mm).

After that, the box was printed using the 3D printer, Flash Forge Creator Pro©, and PLA filament as the printing material. To be able to print PLA the temperature of the nozzle had to be 210ºC and the platform (plate) had to be 110 ºC. The plate and nozzle's locations are shown in Figure 3.2.4. Keep in mind, the temperature of the room where the 3D printer is printing must be at 23 ºC ± 2ºC for the printer to print correctly. The reasoning behind these requirements are summarized in Table 3.2.1.

Figure 3.2.4. The nozzle's and plate's locations in a creator pro 3D printer photo by author.

Table 3.2.1. Ideal temperatures of the nozzle, plate and room where the 3D printer is located and the reasoning behind it

Object	Temperature (°C)	Reason
Nozzle	210	Facilitates PLA filament to melt and pass through the nozzle without hardening inside of the nozzle.
Plate	110	To cool the filament enough to harden. Note that filament has to harden enough to cause interlayer adhesion.
Room	21°C – 25°C	To prevent warping of the sample being printed.

In the beginning of the research, 90% of the print samples warped during the initial printing stage since the printers' location were underneath the cooling vent. After relocating the printers, there was no warping during printing. The samples were printed by having the nozzle excrete 4 mm thick strands, also in this research filament thickness

was not investigated for that the beams were printed at a 100% fill. After taking these steps into consideration the beam was printed and assembled, Figure 3.1.5 shows how the cap and the hollow box combined after printing.

Figure 3.2.5. The first assembled CT beam.

3.3Three-Point Flexural Test.

Flexural strength was defined earlier as the resistance of a member to bending. To do the three-point flexural test, a load is applied at the center of the beam causing a moment envelope along the beam. Figure 3.3.1 represent how a 3-point flexural test is proceeded, the shear and bending moment envelopes caused by the point load, P.

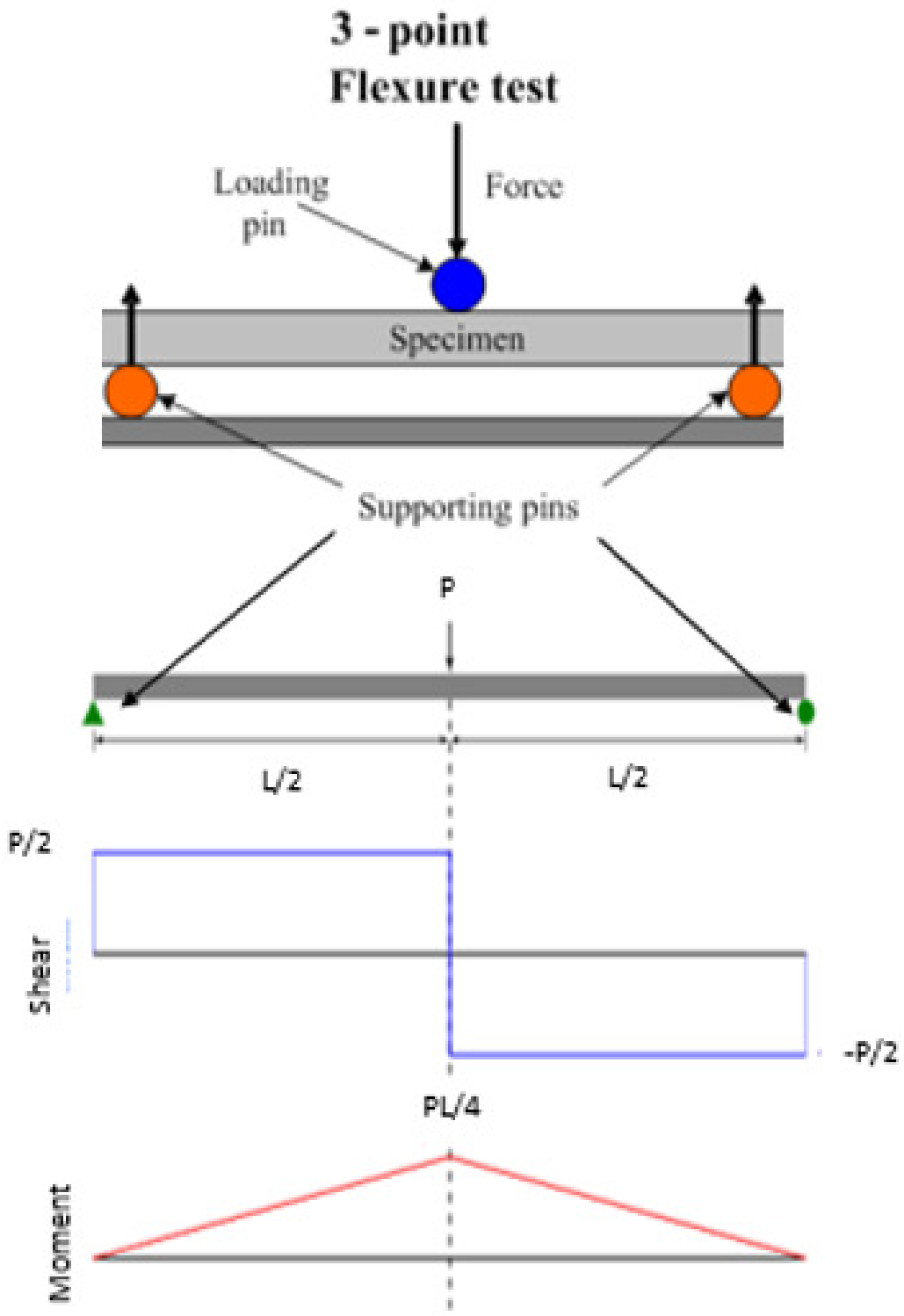

Figure 3.3.1. 3-point flexure test. This illustration was adopted from Kopeliovich, 2017, and modified to present the shear and moment caused by the point load.

The apparatus used to perform the 3-point flexural test was MTS hydraulic actuator which can provide loads up to 50 kN. MTS can be used as flexure testing apparatus, as shown in Figure 3.3.2. The beam was simply supported and tested by applying a point load at the center of the beam. As the beam is being tested the data from the MTS hydraulic actuator was recording simultaneously, providing us with force versus displacement data.

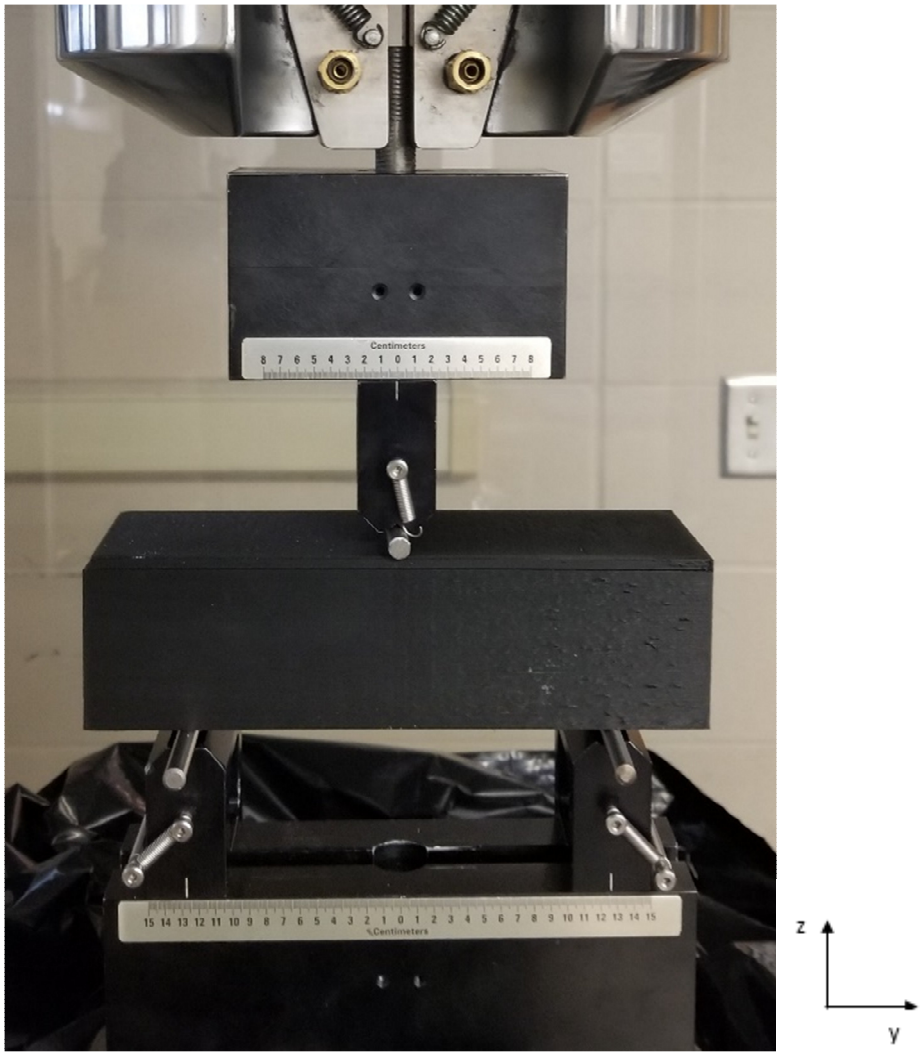

Figure 3.3.2. 3 point flexural testing apparatus setup.

3.4Analyzing the Data

To perform flexural analysis and obtain the flexural properties of the beams the force-displacement data were translated to stress-strain data. To obtain the stress-strain data the ASTM D790, *Standard Test Methods for Flexural Properties of Unreinforced and Reinforced Plastic and Electrical Insulation Material*, was followed.

1) The bending moment was obtained using Equation 3.2

$$M = \frac{PL}{4} \qquad \text{Equation 3.2}$$

Where;

M = the bending moment

P = the applied load

L = the span length between the two supports

2) The flexural stress was estimated for both beams with and without sand. To determine the flexural stress of the hollow beam (no sand) Equations 3.3 was used and to determine the flexural stress of the full beam (with sand) Equation 3.4 was used.

$$\sigma_f = \frac{PLd}{8I} \qquad \text{Equation 3.3}$$

Where;

σ_f = is the flexural stress [Force/Area]

d= is the depth of the beam in the z-direction [Length]

I= is the moment of inertia of the beam [Length^4]

$$\sigma_f = \frac{3PL}{2bd^2}$$ Equation 3.4

3) The flexural strain was calculated using Equation 3.5

$$\varepsilon_f = \frac{6Dd}{L^2}$$ Equation 3.5

Where;

ε_f = flexural strain. [length / length or %]

D= deflection at the center of the beam [length].

4) Flexural stress-strain graphs were then obtained using Excel, having the flexural stress on the y-axis and the flexural strain on the x-axis.
5) The modulus of elasticity in bending was estimated by taking the slope of the linear region in the elastic region of the stress-strain graph.
6) Comparing all the similar samples together and estimating the standard deviation using Equation 3.6

$$s = \sqrt{\frac{(\sum x^2 - nX^2)}{n-1}}$$ Equation 3.6

Where;

S = the standard deviation

x = value of a single observation

X = mean value of the set of observation

n = number of observations

3.5Quality Control

For quality control five samples were printed for every design in this experiment. Since the printer is programmed for extreme accuracy, the samples dimensions matched within 0.01 in. Also the mechanical properties of the beams were almost identical. The difference between the mechanical properties could have been caused by human error.

Research Results and Discussion

To determine the flexural properties of the composite beams. The research was divided into the following continuous cycle.

4.1 Mechanical Properties Analysis

The initial design of the CT beam, Figure 3.2.1, was not ideal during testing. Due to the sand's reaction, Figure 3.1, the walls started to bulge causing the cap to sink in during the 3-point test which made the walls to act like slender cantilever columns, resulting in a low force resistance. Figure 4.1.1 is a force-displacement graph that illustrates the maximum force resisted was 2.6 KN which before failure.

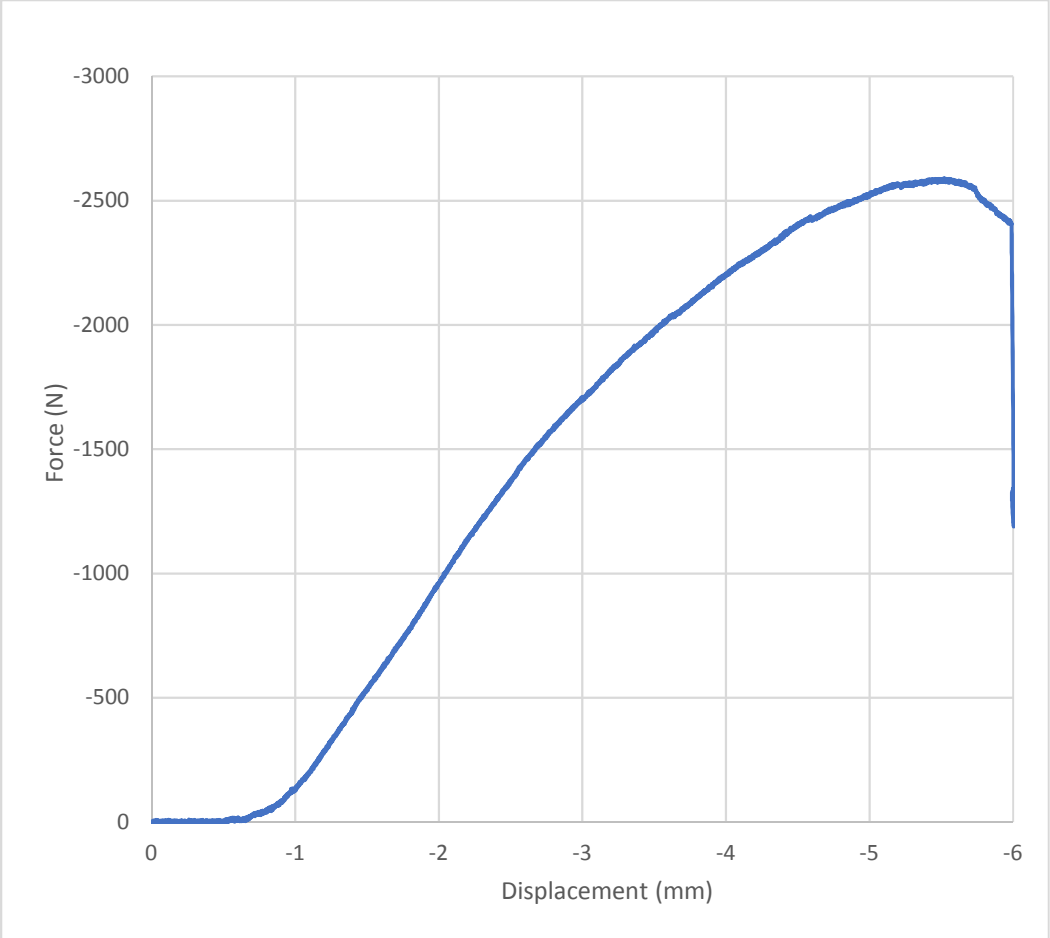

Figure 4.1.1. Force vs. displacement data for beams CT.

Further analysis was performed to determine the flexural properties of the initial beams.

First, Force-displacement data were used to acquire the stress-strain data, Figure 4.1.2.

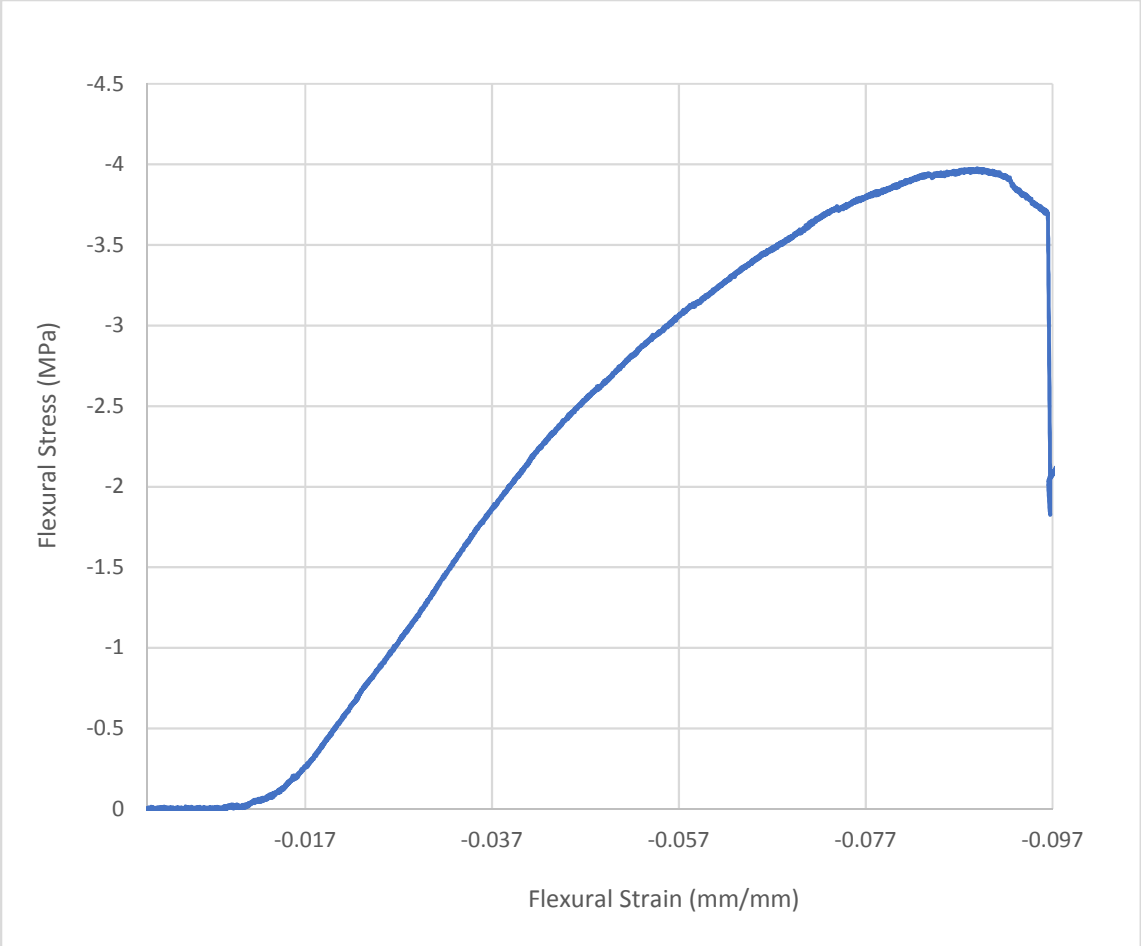

Figure 4.1.2. Flexural stress-strain data for the CT beams.

From the stress strain diagram flexural modulus, flexural strength and strain were determined and tabulated in Table 4.1.1.

Table 4.1.1. Flexural properties of the CT beams with sand including standard deviation (n=5).

Modulus of Elasticity (MPa)	77.0 ± 0
Maximum Force (KN)	2.56 ± 0.0019
Maximum Bending moment (kN-mm)	86.3 ± 36
Maximum Flexural stress (MPa)	3.97 ± 0.002
Maximum Flexural strain	0.097 ± 2.3 E-5

The second set of samples were the CB beams, which were the CT beams rotated 180 degrees about the z-axis, to eliminated the chances of the cap sinking into the beam and that caused the flexural strength to increase, Figure 4.1.3.

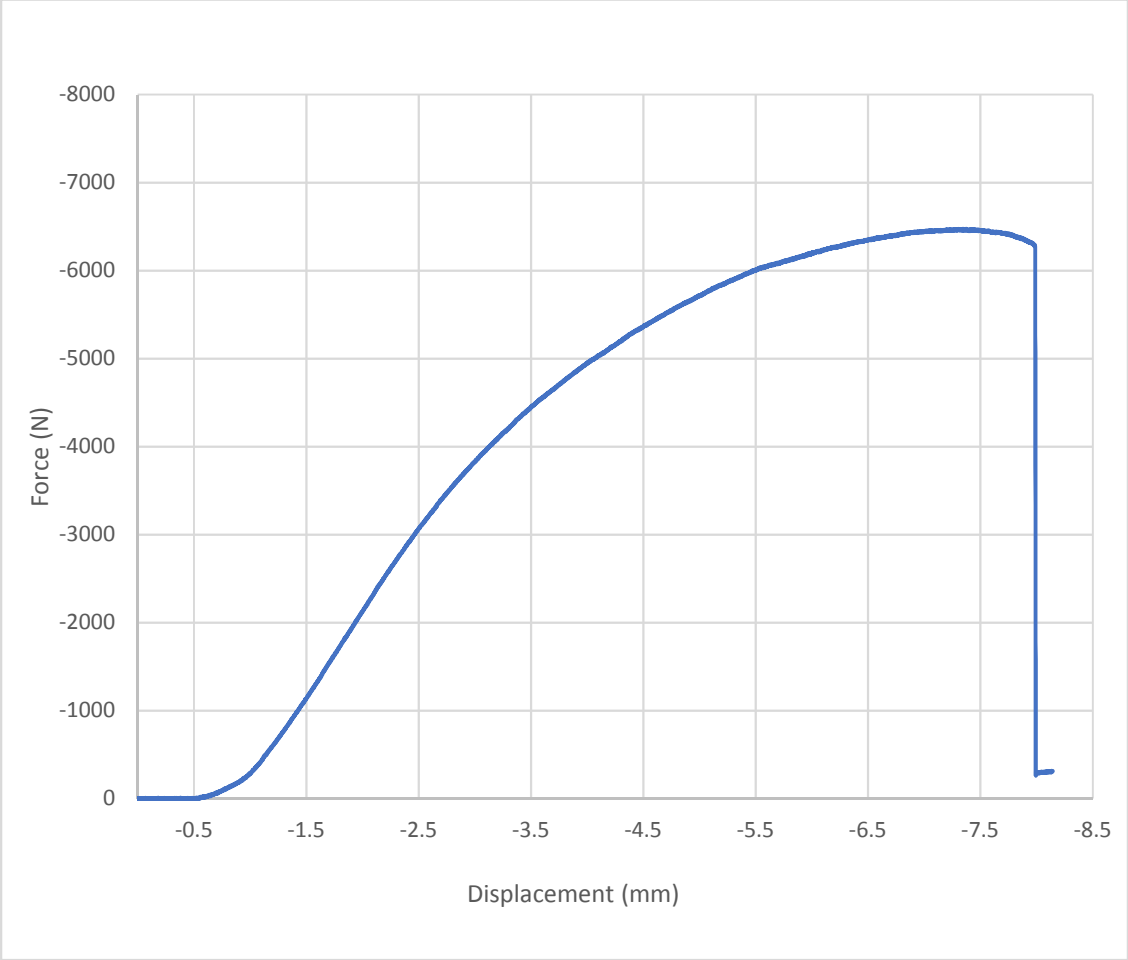

Figure 4.1.3. Force-displacement data for the CB beams.

By changing the beam's orientation the beam gained 160% more force resistance capacity to where it increased from 2.6 kN to 6.5 kN and the effective displacement increased from 6 mm to 8 mm. Effective displacement is the displacement at the center of beam until failure occurs. Failure of the sample in this research is identified to be at a

point where the force has dropped significantly and all at once. Additionally, the mechanical properties of the CB beams were acquired by obtaining the stress-strain data, Figure 4.1.4.

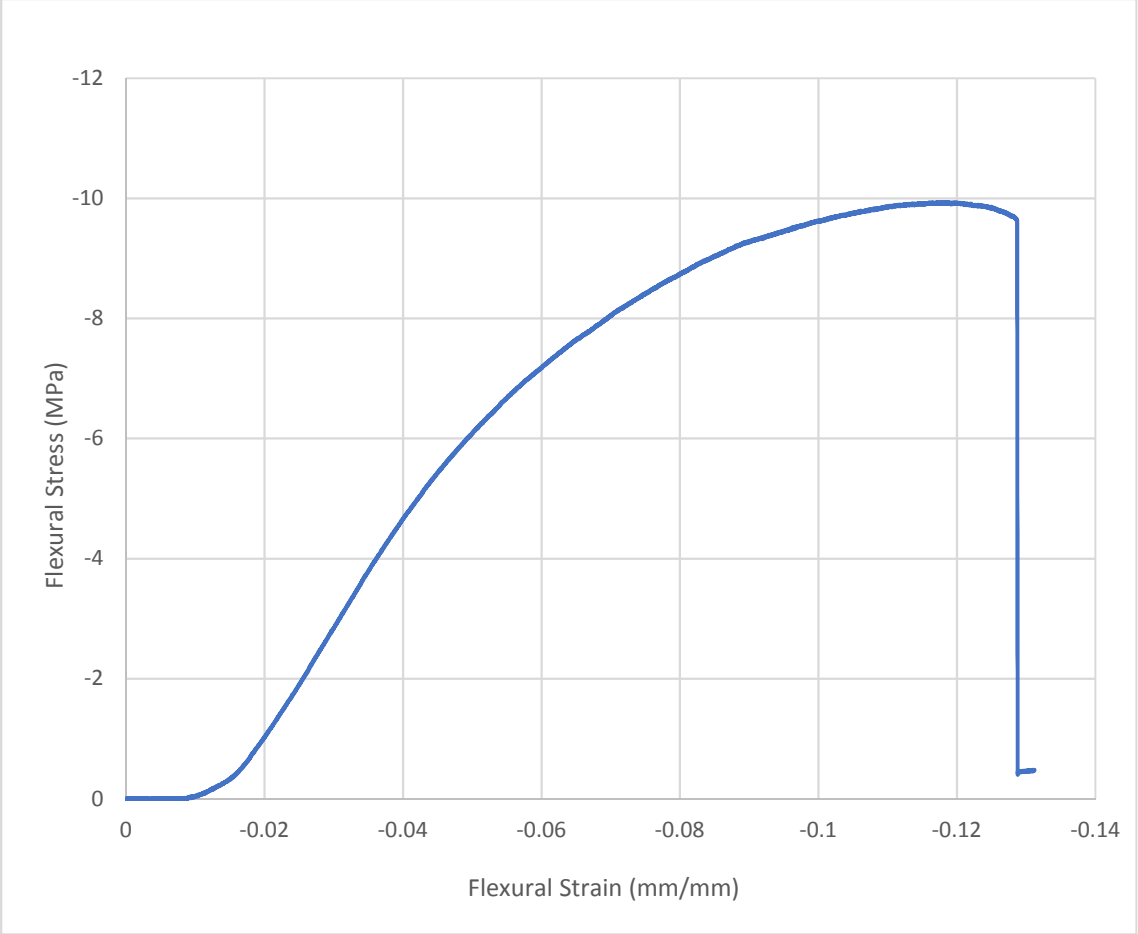

Figure 4.1.4. Stress-strain data for the CB beams.

From the stress-strain diagram, Figure 4.1.4, the mechanical properties of the CB beams were obtained and tabulated in Table 4.1.2.

Table 4.1.2. Flexural properties of the CB beams with sand including standard deviation (n=5).

Modulus of Elasticity (MPa)	182 ± 0
Maximum Force (KN)	6.50 ± 0.19
Maximum Bending moment (kN-mm)	216 ± 6.4
Maximum Flexural stress (MPa)	9.94 ± 0.0003
Maximum Flexural strain	0.13 ± 1.2E-4

To verify if the sand was the factor causing the bulging of the wall, a beam without sand was tested and analyzed. The results of the test are summarized in Figure 4.1.5-6 and Table 4.1.3.

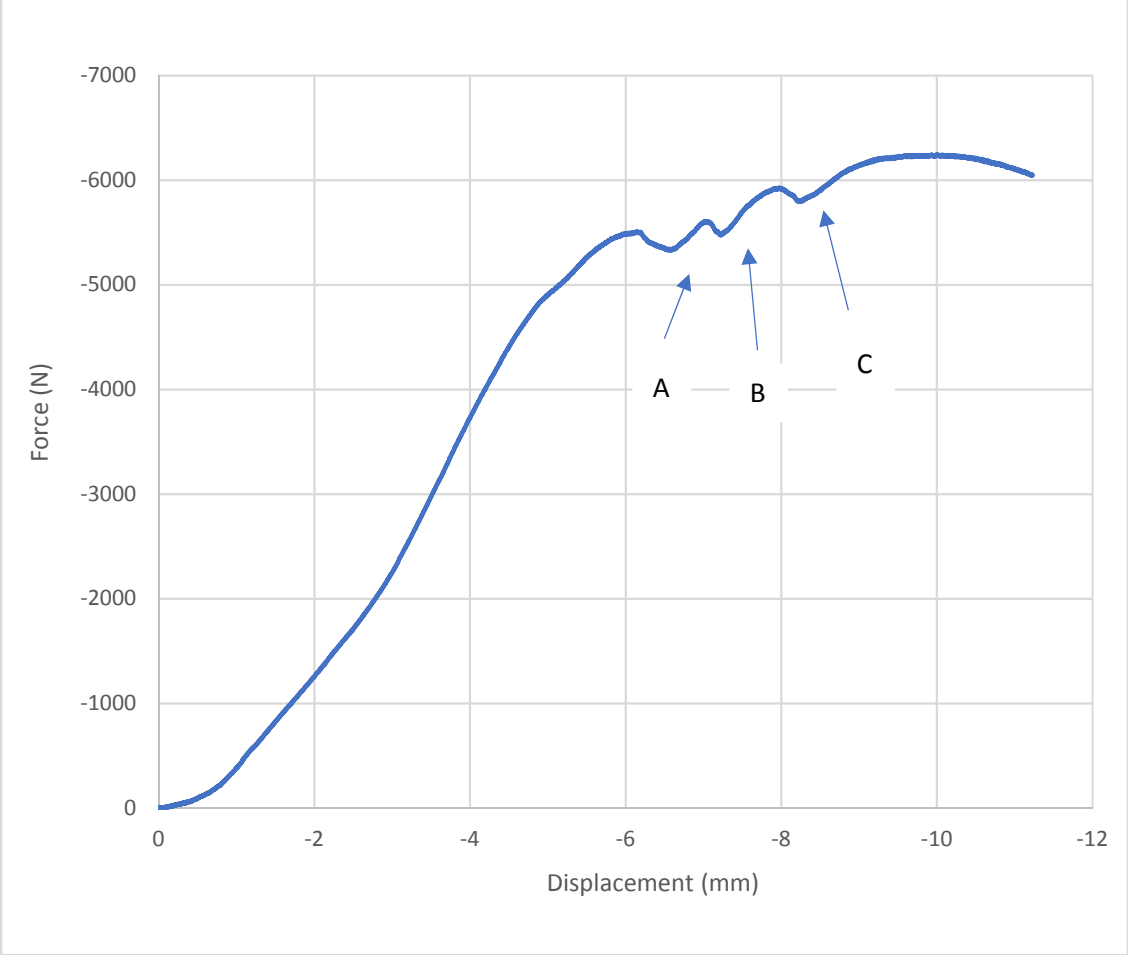

Figure 4.1.5. Force-displacement data for the CT beam with no sand. Point A, first set of

strands fracture, Point B is the second set of strands fracture, and Point C is the third set of strands fracture.

The force-displacement graph (Figure 4.1.5) shows the results of the CT beam with no sand. This verifies that the sand was causing the walls to bulge and act as a cantilever-slender wall. Without the wall bulging the maximum force resisted was 6.28 kN which is 140% increase in force resistance capacity and the displacement almost doubled. Points A-C on Figure 4.1.5 represent points where PLA strands were fracturing but the test was continued until the beam reached failure, the observed failure modes are explained in section 4.2. The mechanical properties were analyzed to see if they were also affected by the presence of sand within the beam.

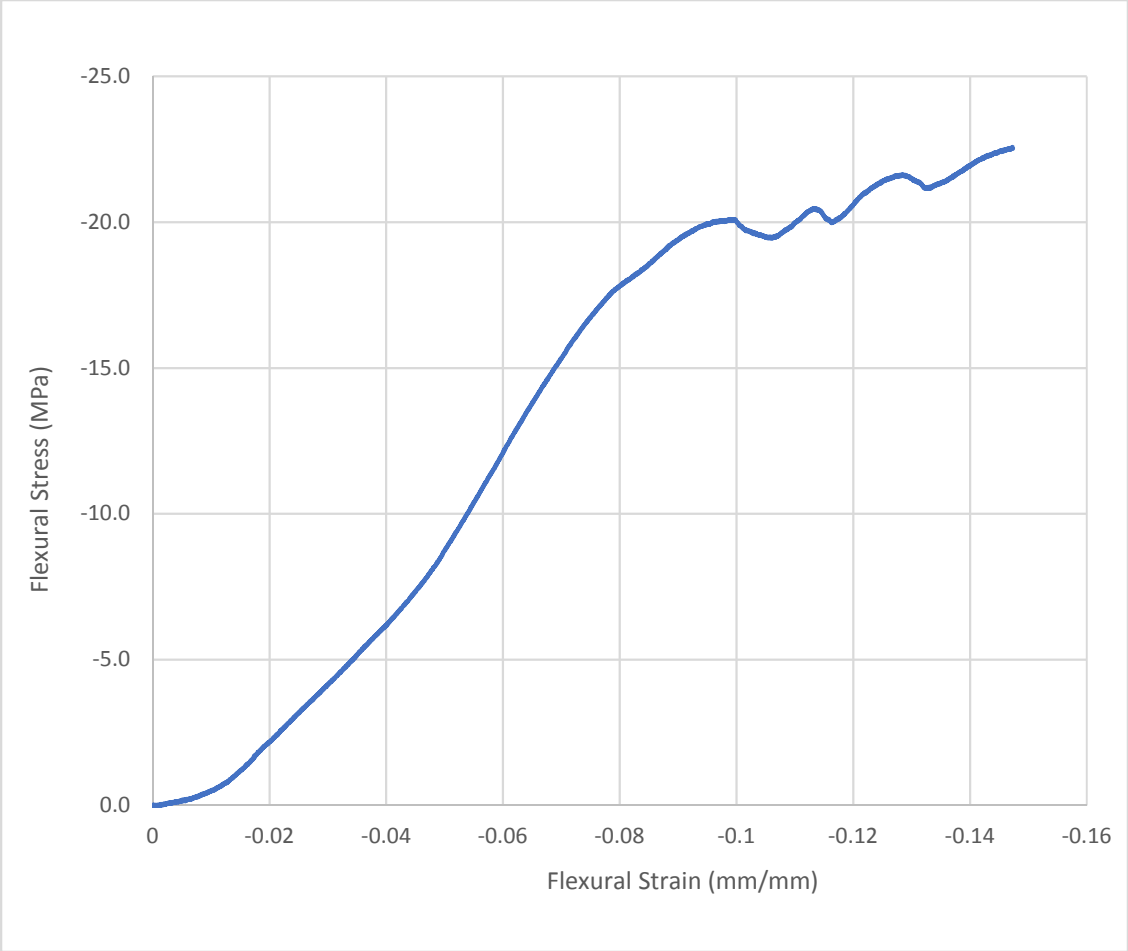

Figure 4.1.6. Stress-strain data for the beam with no sand.

From the stress-strain diagram the mechanical properties of this beam were obtained and tabulated in Table 4.1.3

Table 4.1.3. Flexural properties of the beam with no sand including standard deviation (n=5).

Modulus of Elasticity (MPa)	324 ± 0
Maximum Force (KN)	6.28 ± 0.002
Maximum Bending moment (kN-mm)	206 ± 4.2
Maximum Flexural stress (MPa)	22.6 + 0.0019
Maximum Flexural strain	0.15 ± 0.02

The reasons behind the significant difference in the stress value was because the effective area of the beam has decreased significantly and stress is inversely proportional to the effective area. Additionally, the increase of force resistance capacity caused the stress to increase even more.

Due to the overall improvement of the second set of samples and the proof that the sand contributed in failing the beam. A new design was done which excludes the cap entirely. The second design was a beam with thicker walls than the initial beam design and with a filling hole on top instead of a cap, Figure 4.1.7. Having a filling hole eliminates any chances of the walls acting as cantilever columns which would increase both stability and resistance of the beam.

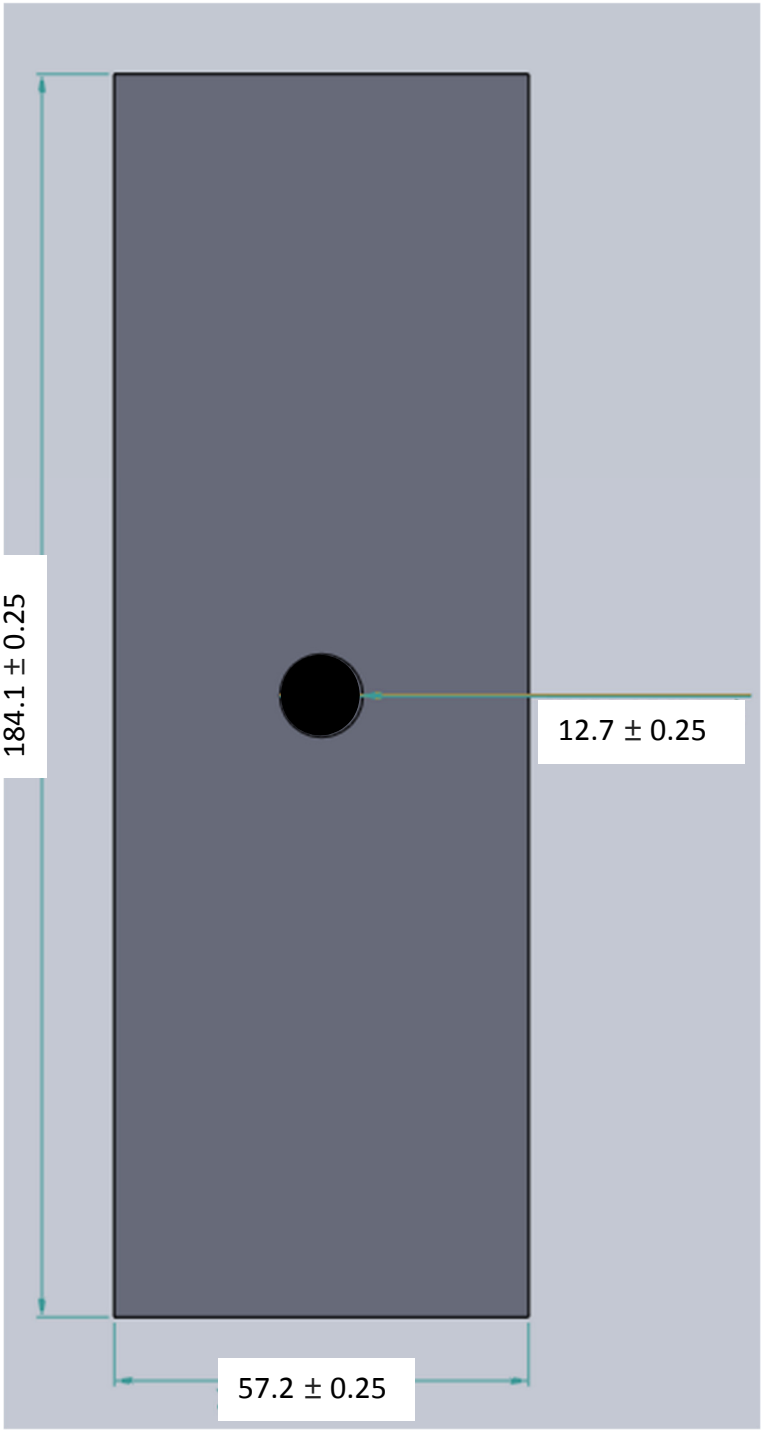

Figure 4.1.7. Top view of the new design beams' (NC beam) dimensions (mm).

The filling hole is located at the center of the beam and has 0.5 in diameter. Having a filling hole decreased the sand filling and packing efficiency. The Unimin sand was

packed by vibration, and due to its grain size, packing by vibration was sufficient. The design improvement provided us with vital information that may lead to further investigation in future researches regarding the PLA interlayer adhesion resistance to the shear forces.

Figure 4.1.8, represents the force-displacement data of the new design and how the force resistance capacity have increased in comparison to CT and CB beams.

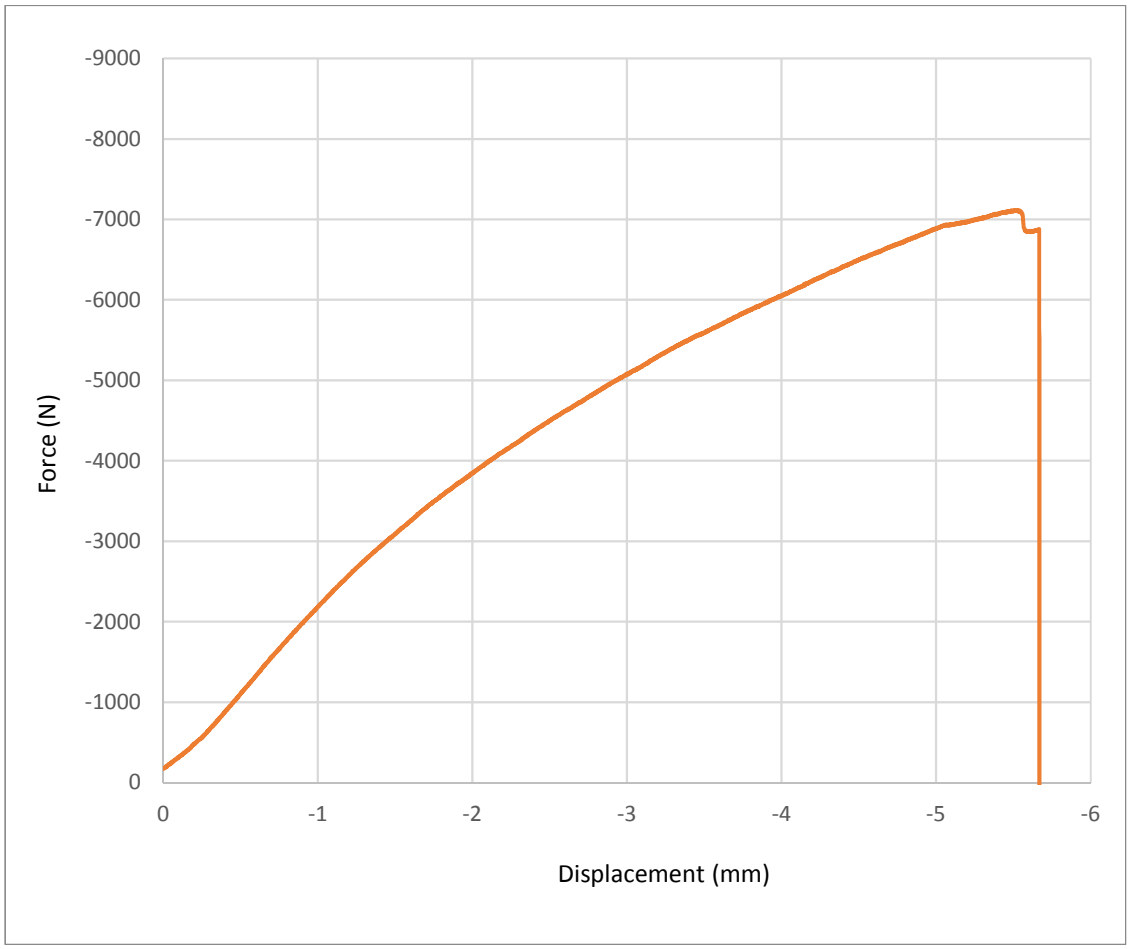

Figure 4.1.8. Force-displacement data of the NC beam with sand.

The maximum force resisted by the NC beam is 7.15 kN which is a 10% increase from the CB beam force resistance, but there was a decrease in displacement. From the force-displacement data the following stress-strain graph was obtained, Figure 4.1.9.

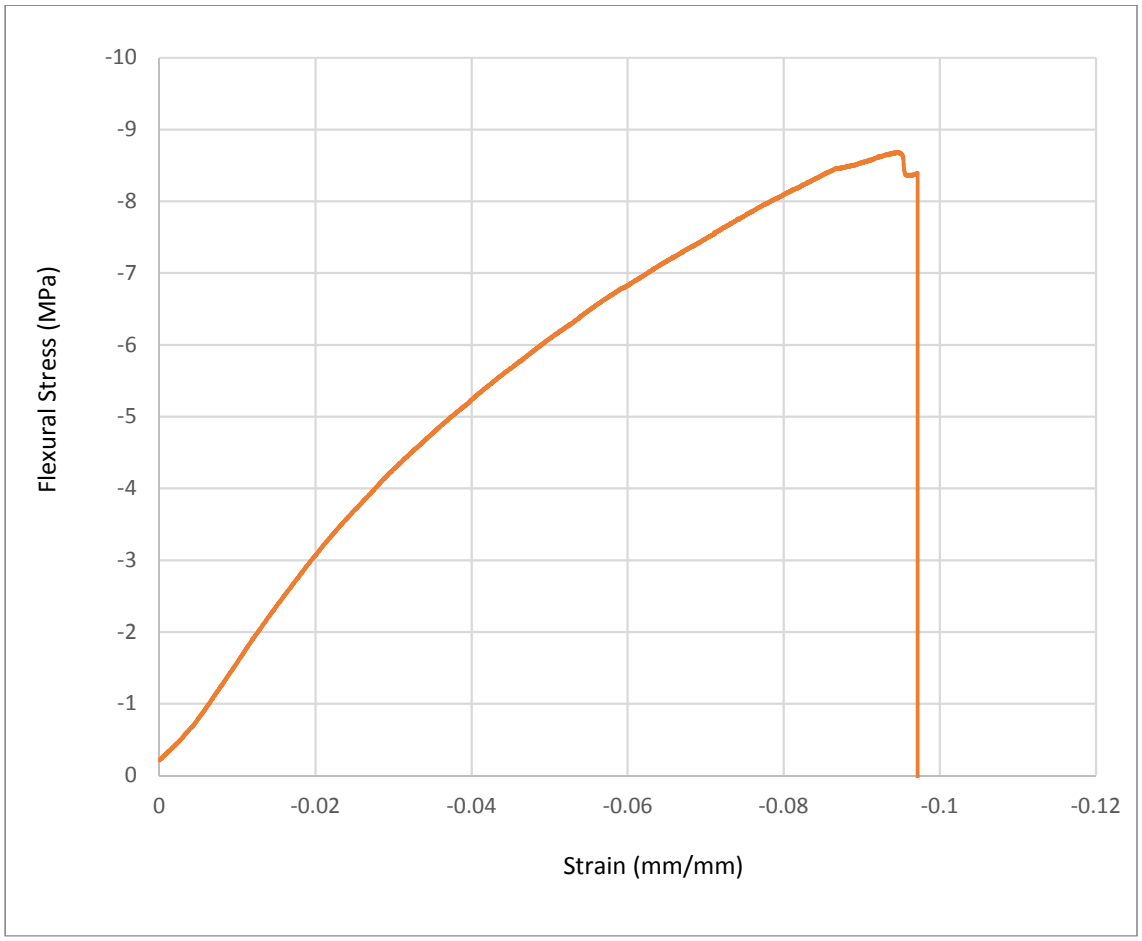

Figure 4.1.9. Stress-strain data of the NC beam with sand.

From the stress strain data the mechanical properties in table 4.1.4 were acquired:

Table 4.1.4. Mechanical properties of the NC beams with sand including standard deviation (n=5).

Modulus of Elasticity (MPa)	151 ± 0
Maximum Force (kN)	7.11 ± 0.027
Maximum Bending moment (kN-mm)	237 ± 0.91
Maximum Flexural stress (MPa)	8.68 ± 0.013
Maximum Flexural strain	0.102 ± 0.01

After obtaining the mechanical properties for the beam, the beam was investigated to check if it is more efficient without sand included. Figures 4.1.10-11 and table 4.1.5 summarize the mechanical properties of the beam with no sand.

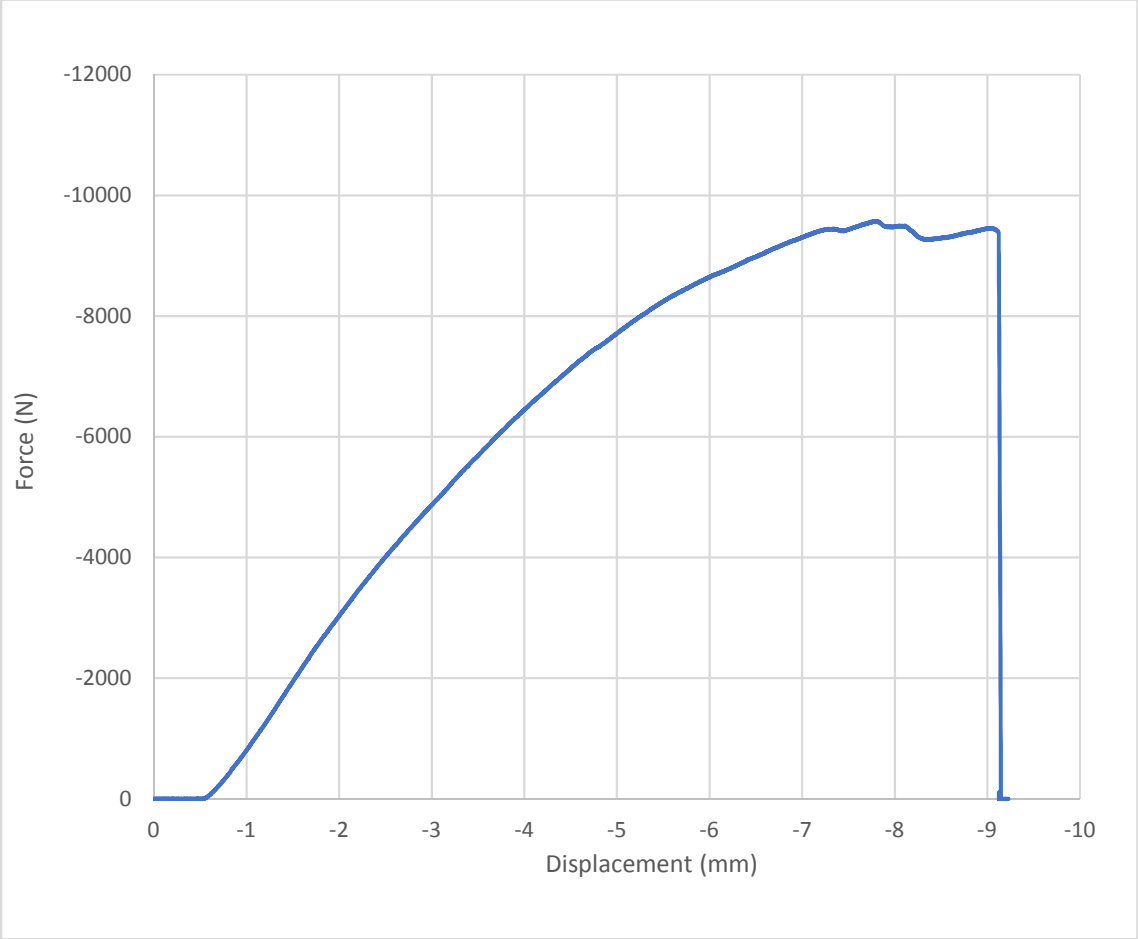

Figure 4.1.10. Force-displacement data for the NC beam with no sand included.

The force-displacement data shows that the NC beam can withhold more load when sand is excluded, where the force resistance increased by 34%. Additionally, the displacement increased by 50%. After that, stress-strain data were obtained and summarized in Figure 4.1.11 and Table 4.1.5

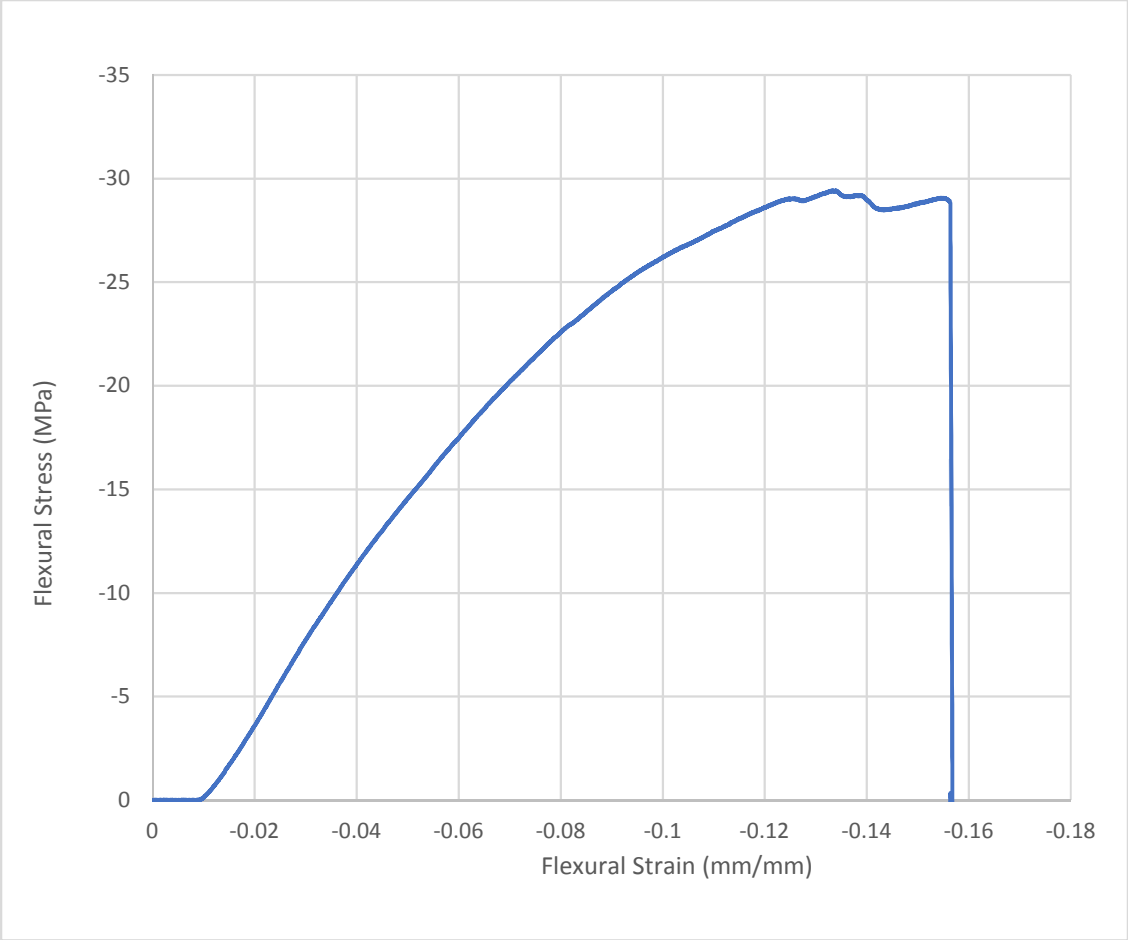

Figure 4.1.11. Stress-strain data for the NC beam with no sand included.

Table 4.1.5. Mechanical properties of the NC beam without sand including standard deviation (n=5).

Modulus of Elasticity (MPa)	406 ± 0
Maximum Force (kN)	9.58 ± 0.031
Maximum Bending moment (kN-mm)	319 ± 0.95
Maximum Flexural stress (MPa)	29.4 ± 0.041
Maximum Flexural strain	0.157 ± 0.003

From the data presented it can be concluded that, eliminating the cap and making the walls thicker would increase the beam's capacity of withstanding bending and loading.

To assess the accuracy of the 3D printer, the mechanical properties of similar samples were compared. Figure 4.3.1 and Table 4.3.1 illustrate a force-displacement data comparison between two NC beams.

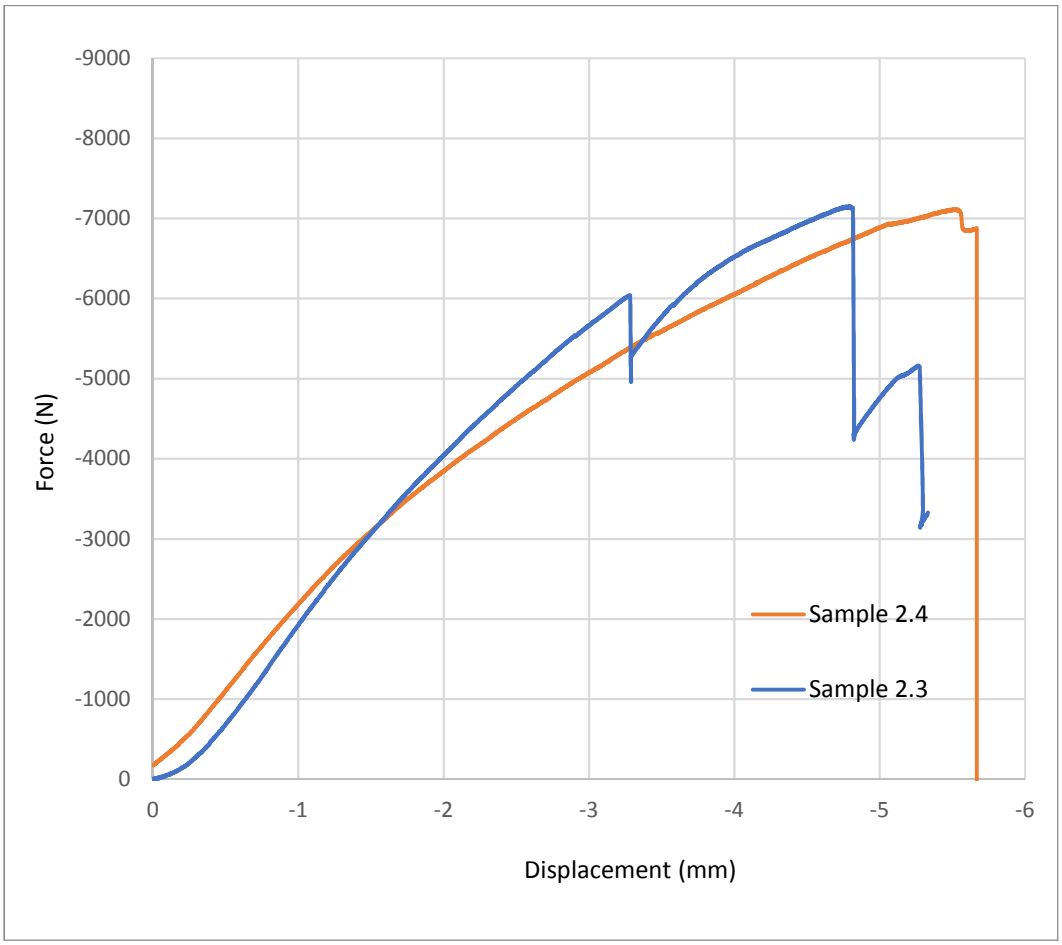

Figure 4.1.12. Comparison of two different samples of the same design.

Table 4.3.1. Comparison of maximum force and displacement of the two samples.

Sample	2.3	2..4	% Difference
Maximum force (N)	7150	7110	0.56%
Displacement at failure (mm)	5.3	5.6	5%

The reason behind the slight difference of the two samples could have been aging of the samples. Due to the minimal knowledge of the aging process, it was not taken into consideration when the samples were printed and for that the time and date of the printing process were not noted. Human and machine errors could have affected that as well.

4.2 Failure Modes

Flexural failure is caused by the tension load acting on the bottom side of the beam, causing flexural-cracks to form which eventually causes the beam to fail. Flexural cracks are shown in Figure 4.2.1.

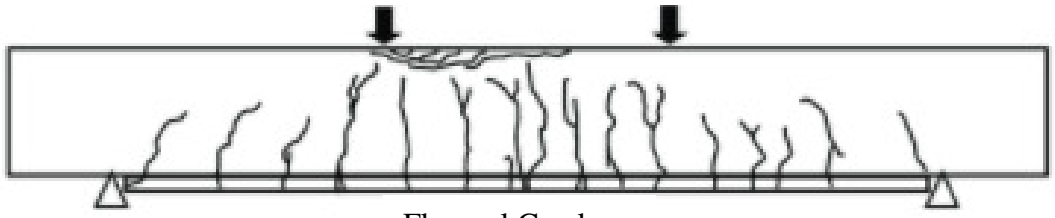

Figure 4.2.1. Schematic of cracks caused by flexural loading (Zhang, D.)

To identify the stress occurring during the three-point testing for this research, a sample of clayey soil at optimum moisture content was placed and packed in the box beam then tested. This allowed us to identify the failure mechanism of the beam samples.

Figure 4.2.2. Flexural cracks on the extracted clay sample.

Point A in Figure 4.2.2 represent flexural cracks developing along bottom side of the beam. Point B represent the PLA strand failure causing a layer to shear and move horizontally due to the weak interlayer adhesion and that is why the flexural cracks do no go past the horizontal line that is represented as B. This shows why the beams have higher capacity when soil is not added in the beam.

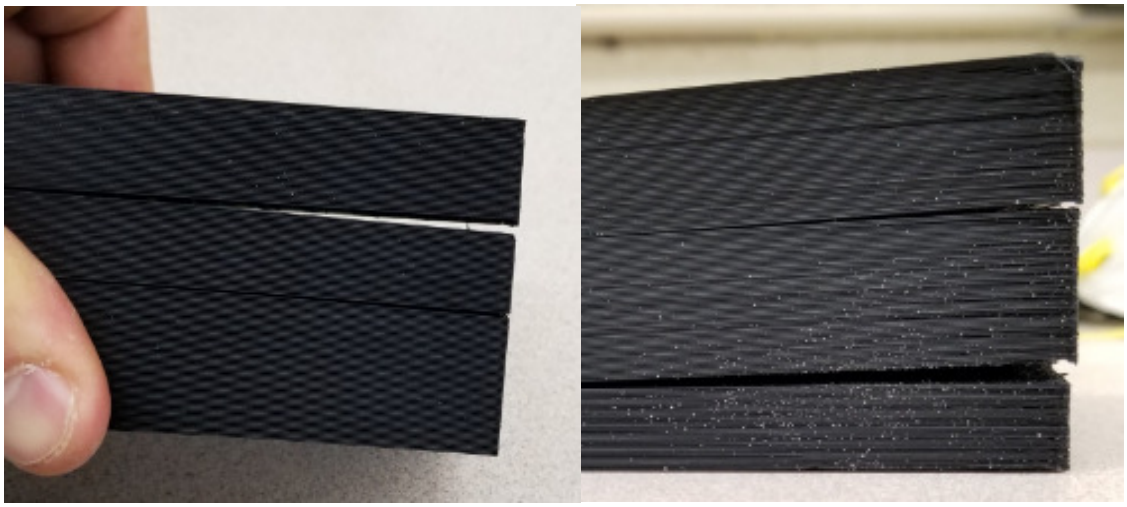

Figure 4.2.3. Interlayer adhesion failure. A failed CB beam on the left and a failed NC beam on the right.

Figure 4.2.3 represents two different samples that had an interlayer adhesion failure in the presence of sand. Note that, in Figure 4.2.3 the cracks were exaggerated for the readers to

be able to see them, during testing the layers move horizontally which causes the interlayer adhesion failure.

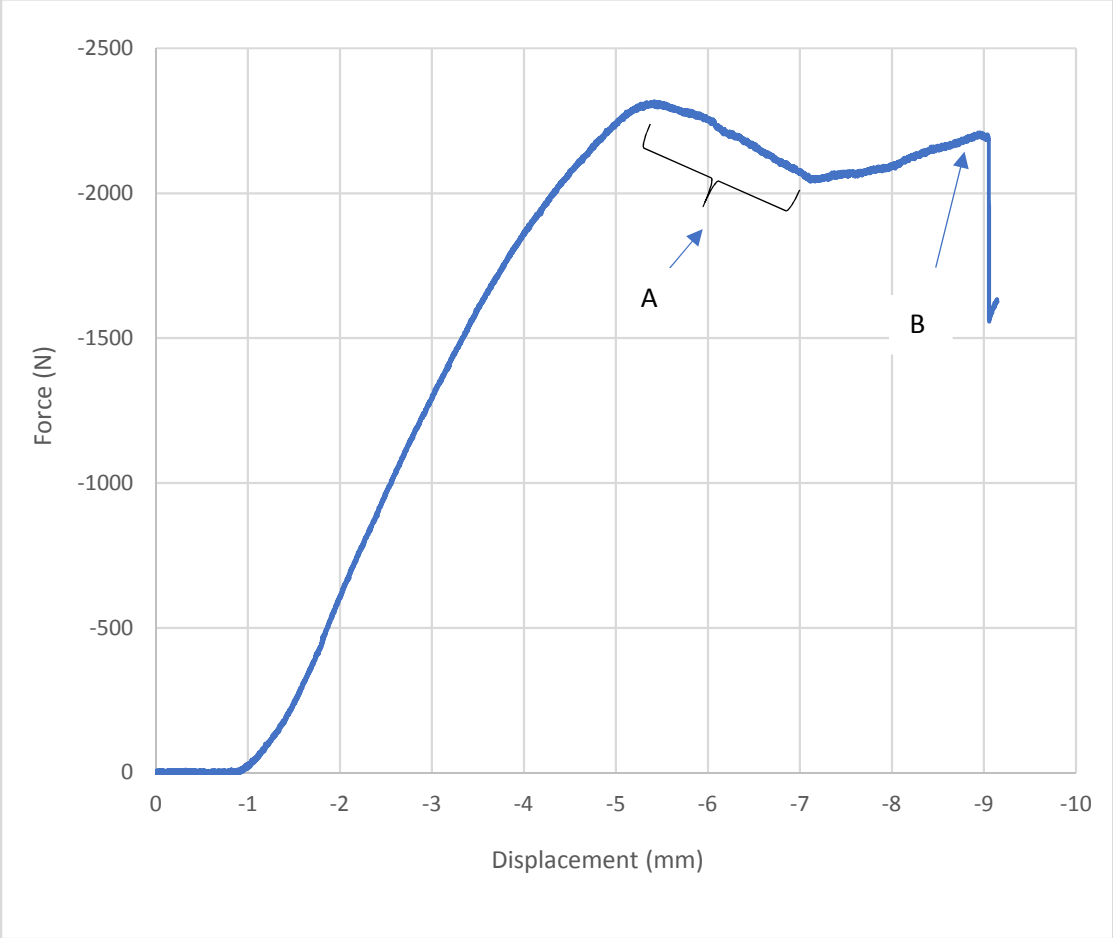

Figure 4.2.4. Interlayer adhesion failure of the CT beam with sand.

From Figure 4.2.4 one can conclude that during the interlayer adhesion failure the beam's force resistance decreases, as shown in point A, then gains back some capacity, point B, and the cycle continued until the beam completely fails.

When the sand was not added in the beam, the beam had a brittle flexural failure. Brittle failure can be defined as a sudden complete failure, Figure 4.2.5 displays the beam immediately before the beam failed.

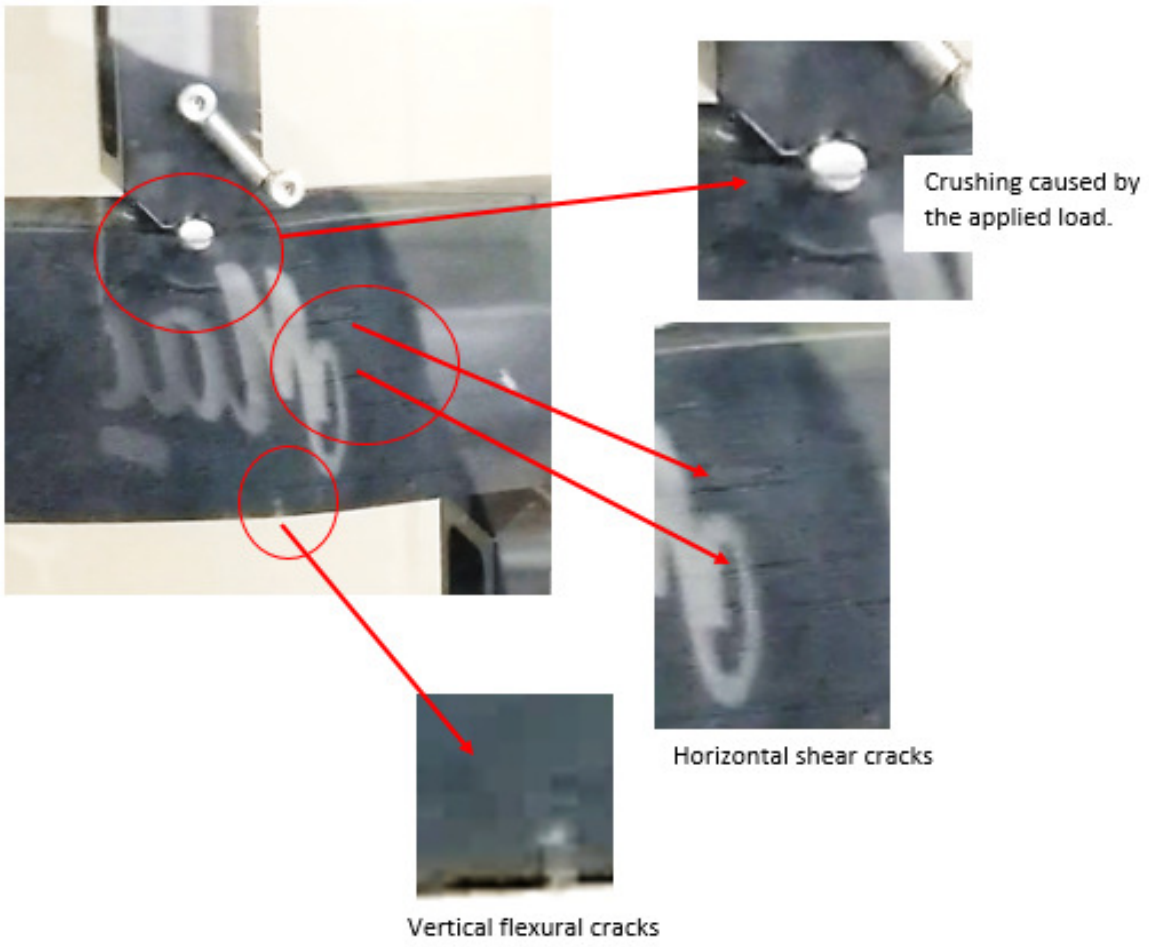

Figure 4.2.5. Beam orientation right before failure.

Figure 4.2.5 a screenshot of a video obtained during testing showing different crack along the beam. Due to the brittle failure of the beam, a protective glass door was in the way which caused the ambiguity of the picture. Shortly after this picture was taken the beam completely collapsed, Figure 4.2.6. Additionally, The failure observed in this scenario is similar to unreinforced timber beam flexural failure.

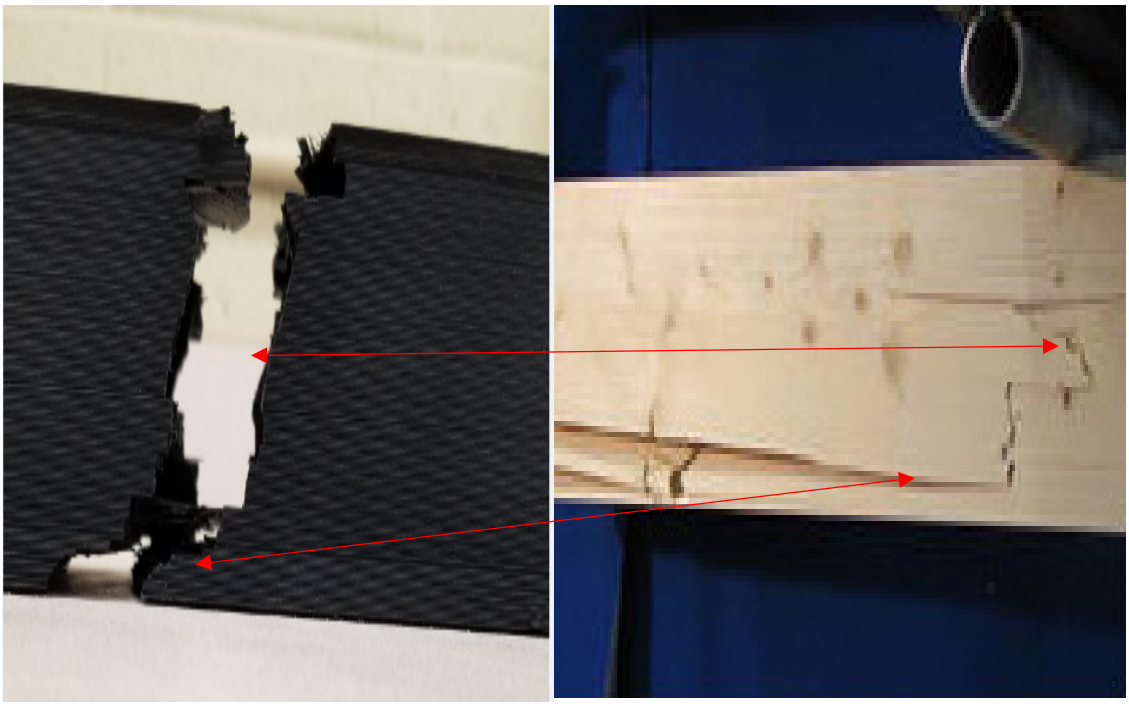

Figure 4.2.6. Beam after the brittle failure. Timber beam picture was adopted and modified from (www.hb.bgu.tum.de)

The brittle failure can also be represented by the by the stress-strain graph of the beam with no sand. Figure 4.2.7 is a perfect illustration of the brittle failure where at point A you can conclude that there excessive cracks developing and a point B a sudden failure occurring.

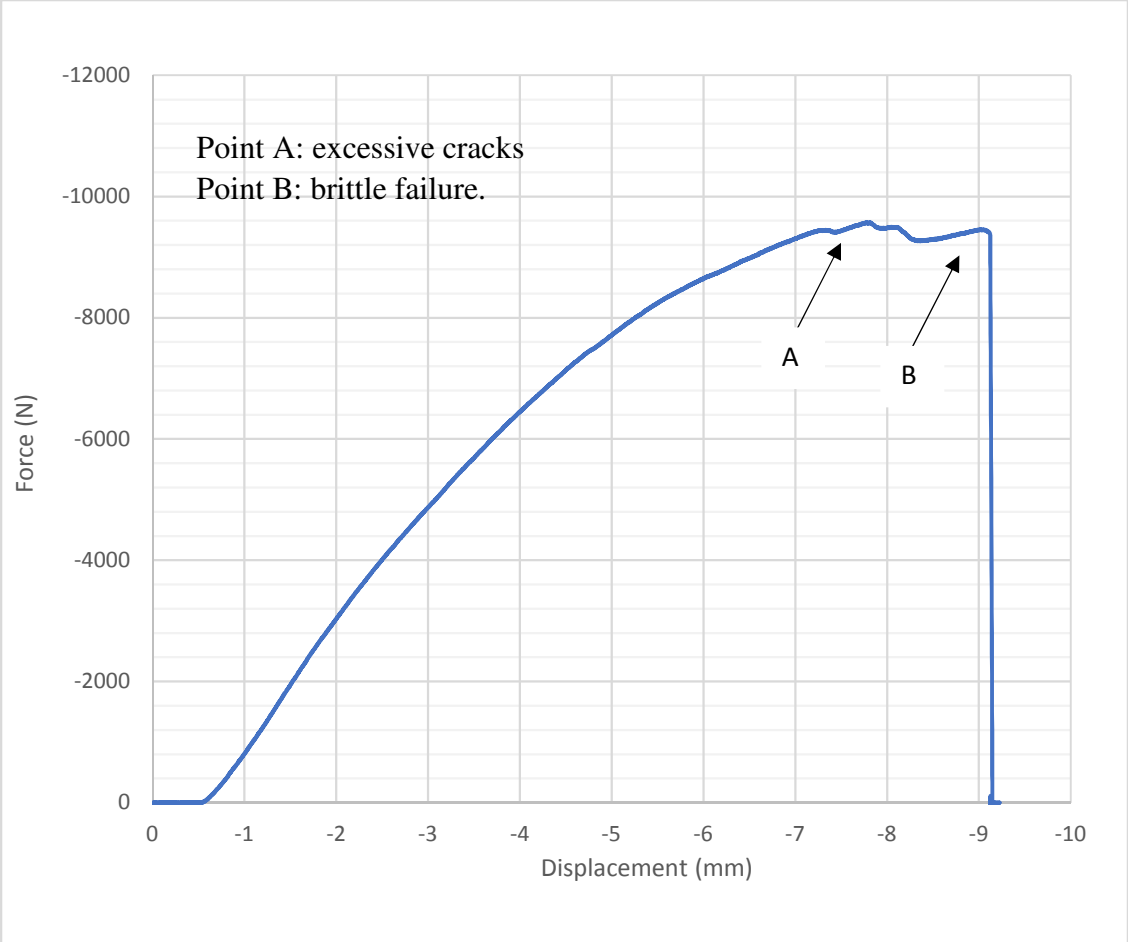

Figure 4.2.7. Flexural failure representation of the NC beam with no sand. Point A represents excessive cracking and point B represent brittle failure.

4.3 Design Comparisons

After ensuring quality control the mechanical properties and force resistance the following bar charts are used to compare between all the beams.

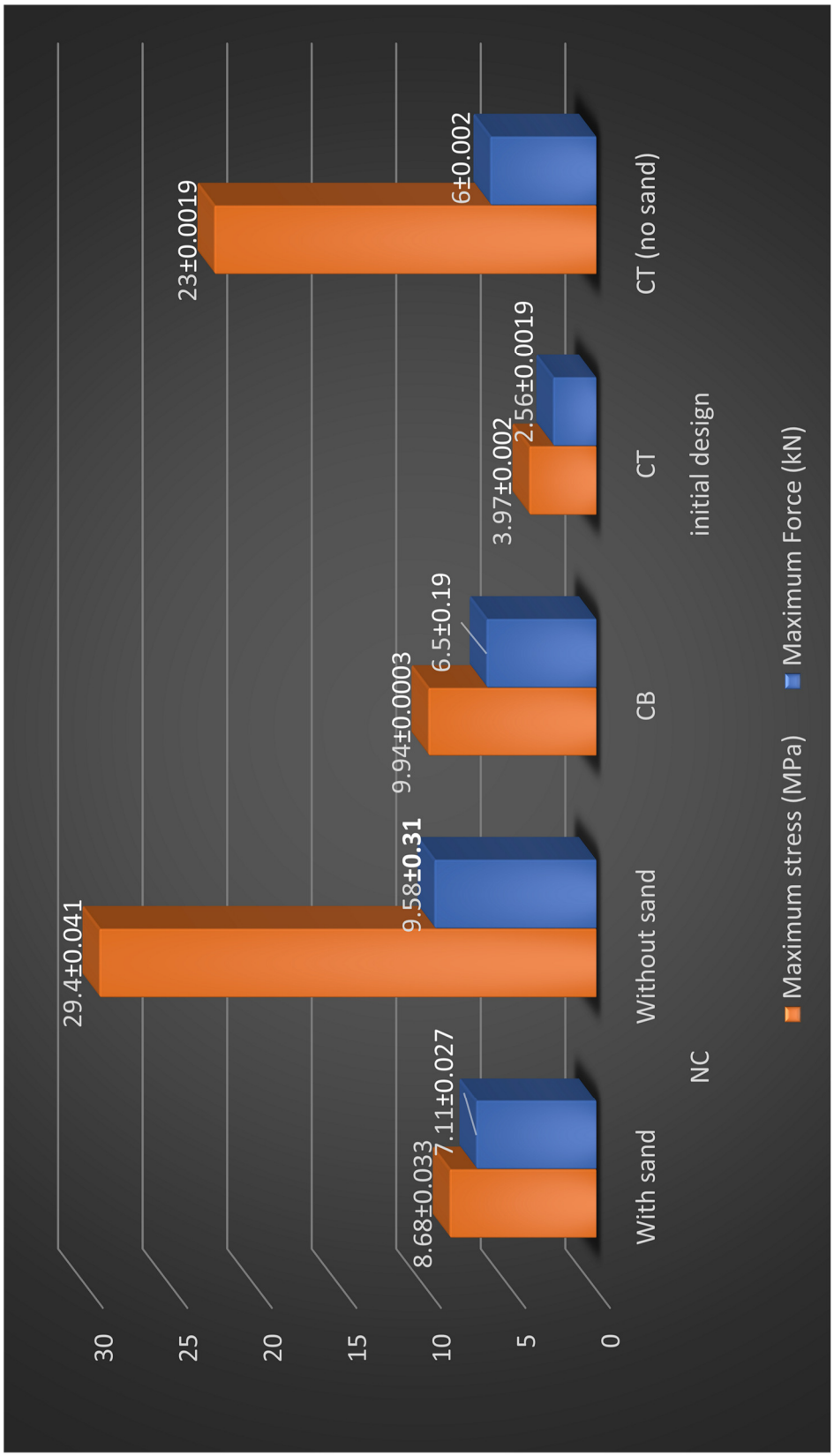

Figure 4.3.1. Force and stress comparison between all the beam designs.

Figure 4.3.2 illustrate how interlayer adhesion failure caused by the sand affects the force resistance capacity of the beam, since the beams without sand had higher load resistance capacity than the beam with sand. After comparing the force resistance capacity, the flexural stress capacities were compared. It is concluded that beams with no sand have a higher stress capacity that those with sand. Although the beams without sand can carry more load and withhold more stress they are not as safe as the beams with sand due to the brittle failure mode of the beams without sand.

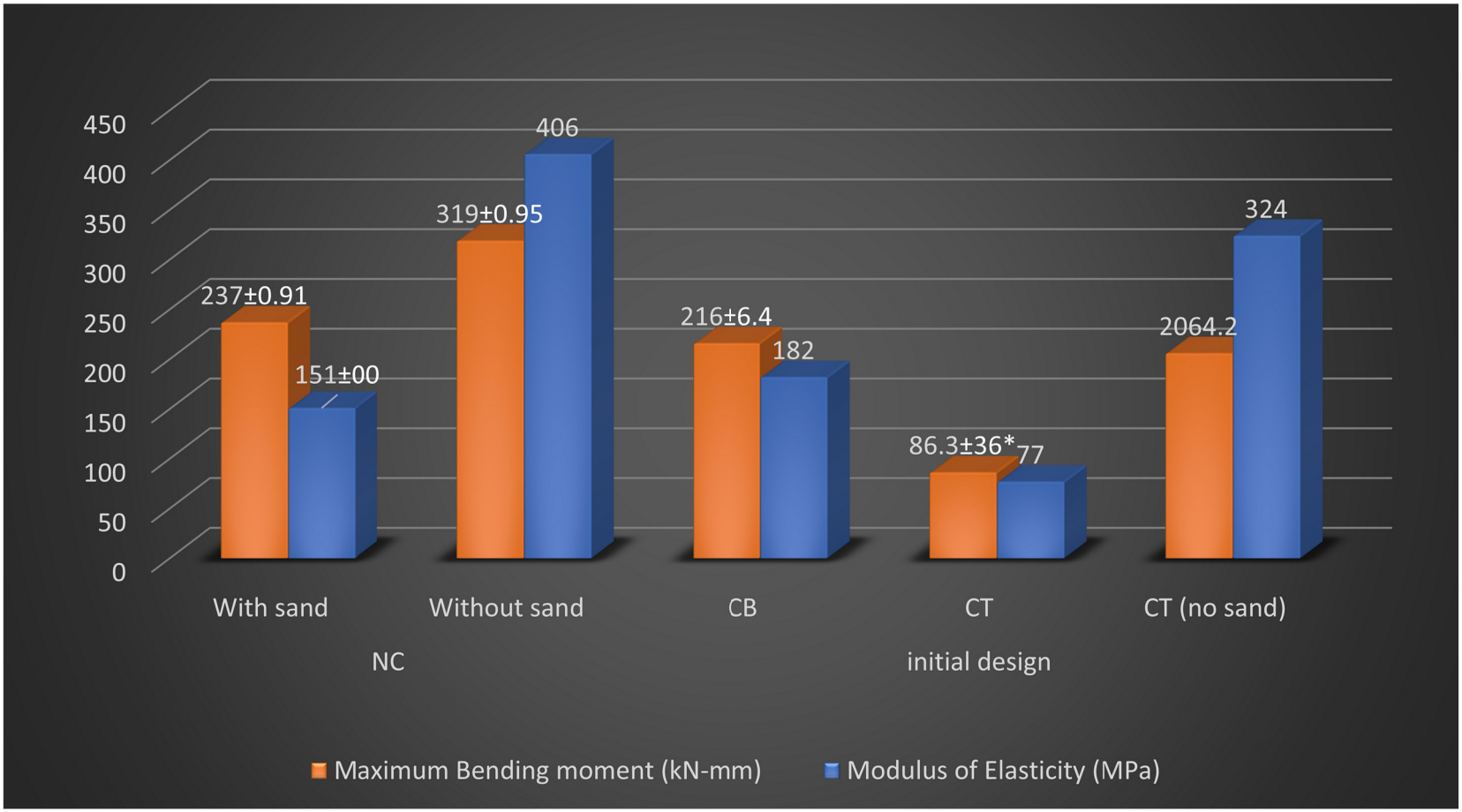

Figure 4.3.2. Bending moment and modulus of elasticity comparison

Given to the linear relationship between the applied force and bending moment it is of no surprise that the maximum bending moment of the beams follow the same trend as the force resistance capacity. The modulus of elasticity, is higher for the beams with no sand than those with sand.

Finally, failure modes of beams are different. When filling the beam with sand, an interlayer adhesion failure occurs. Whereas, when the beam is not filled with sand, a brittle failure occurs.

Conclusion

Due to the poverty level in the world and the rising plastic waste. Utilizing plastics as structural members would solve two problems, since it is affordable and would dramatically decrease the plastic waste. In this research, composite beams made of plastic and fine soil were designed, tested and analyzed to see if the design would be sufficient and safe as a structural beam. Beam is controlled by flexural properties due to the orientation of the load on the member. To perform flexural testing and analysis of the beams, ASTM D790 was followed. In this research, three beam designs were developed and tested where the newer designs were improvements of the previous designs. Design improvement were developed in order to address the undesired failure modes like the interlayer adhesion failure. After testing and comparing the flexural properties of the beams, we can conclude that beams without the fine soil have a higher flexural capacity than the beams with the fine soil, which caused the vertical point load to transition into a horizontal load within the soil causing the interlayer adhesion failure. Additional research is necessary before it is implemented as a real structural member.

Future Recommendations and OLC projects

The following are recommendations for future research:

1) Investigation of aging effects on 3D printed beams, we came to realization that aging of the samples after printing affect the mechanical properties of the samples. How aging of the 3D printed PLA samples came into realization is when comparing two CT beam samples both with no sand with only difference being the time between printing and testing of the two samples. One of the samples was printed and tested within 24 after printing was completed, and the other sample that was printed 14 days prior to testing. The two samples' force-displacement data and stress strain data were compared and are provided in Figure 6.1. Note that the 24 hour sample data was given an offset of 1.5 mm.

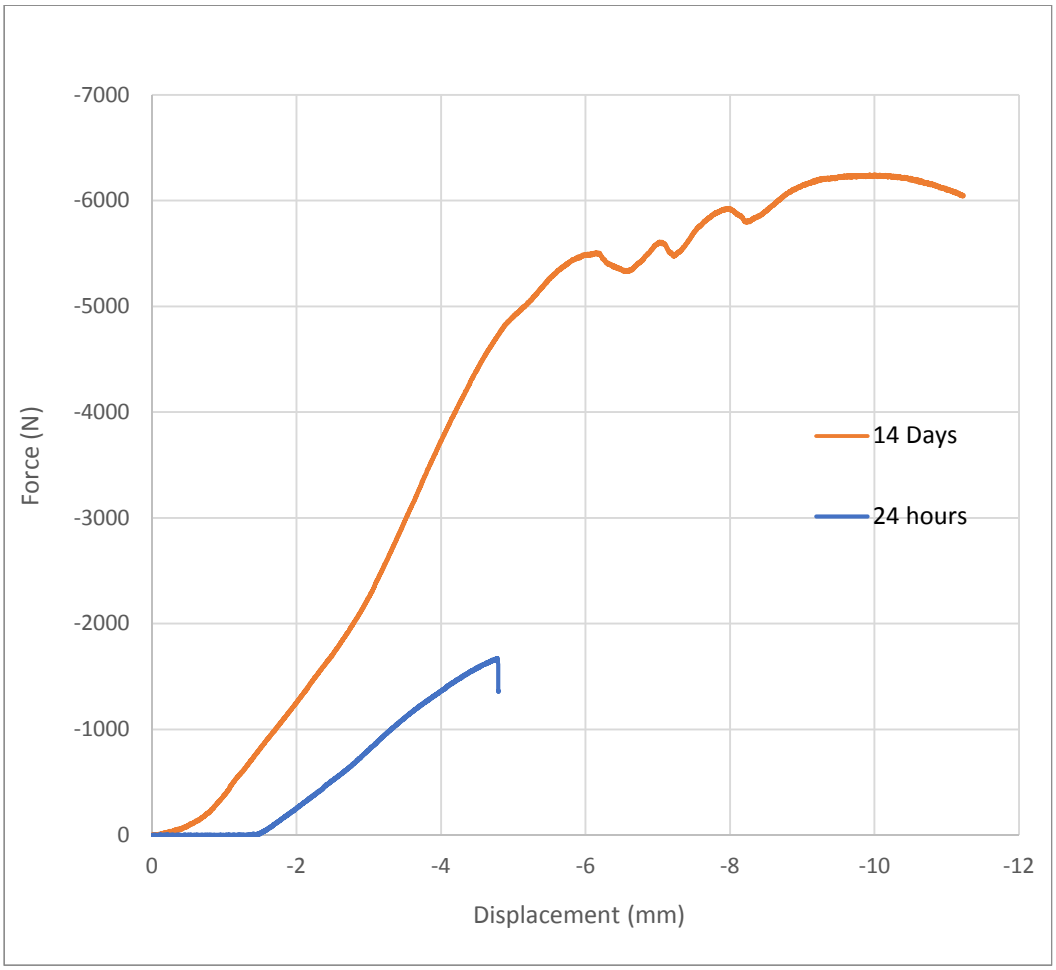

Figure 6.1. Force-displacement comparison between two CT beams one that aged for 14 days and the other CT beam only aged for 24 hours before testing.

Figure 6.1 illustrates how aging plays a major factor in increasing load resisting capacity and the elasticity of the beam. Where the maximum force of the 14 day sample is 294% higher than the maximum force of the 24 hour sample. Also the displacement increased by 220%. Figure 6.2, shows how aging increased the stress by 275%.

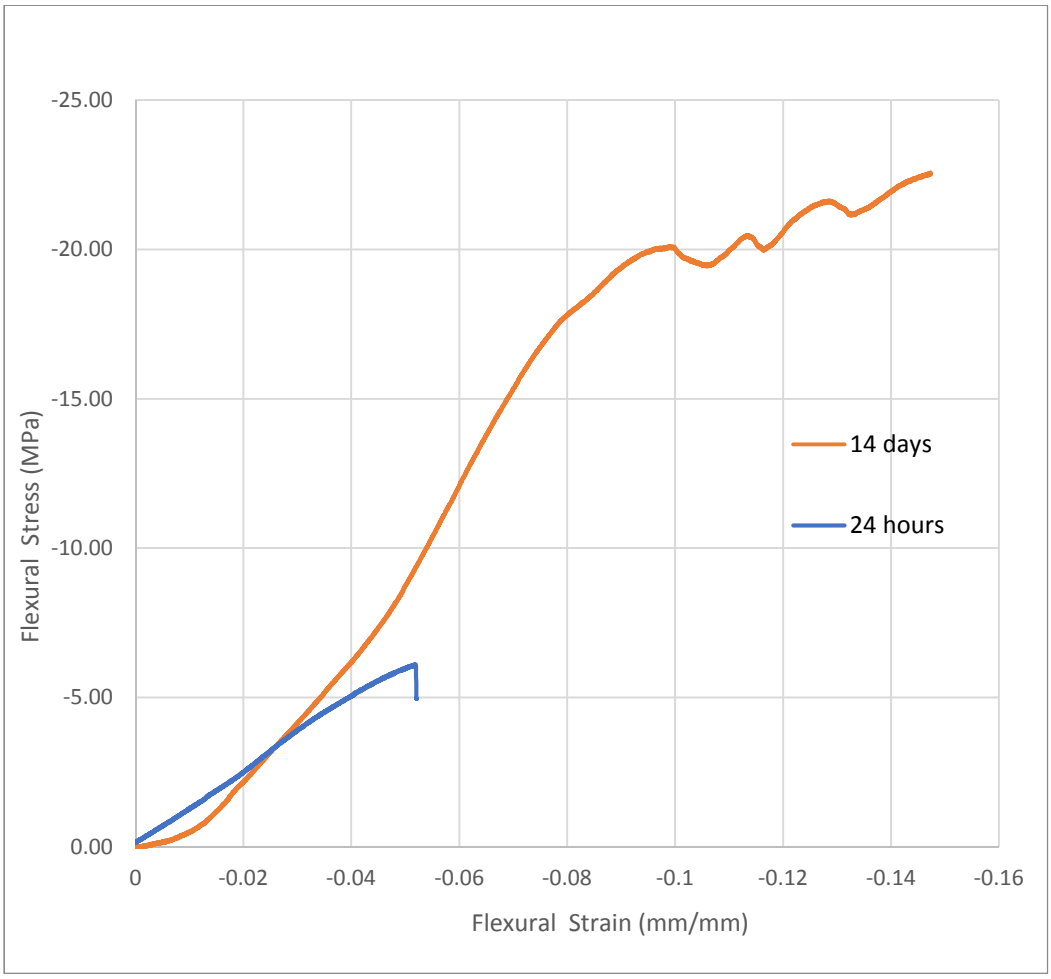

Figure 6.2. Stress-strain data comparison between two CT beams one that aged for 14 days and the other CT beam only aged for 24 hours before testing.

Since aging of the samples was not included in the objectives of this research it was not further investigated due to time restrictions. Also no research has been performed on aging of 3D printed samples. For that, it is recommended for future research.

2) Using material that would prevent interlayer adhesion failure. For example, Fiber-Reinforced Plastic (FRP) can be used as a reinforcement which would prevent the interlayer adhesion failure and will increase the capacity of the designed beams.

FRP comes in many forms, the form that would work with these beams would the ones that wrap around the beam.

3) Improving the design of the beam, by adding a third wall within the beam similar to a concrete block, Figure 6.3. Adding a third wall may increase the flexural capacity of the beam.

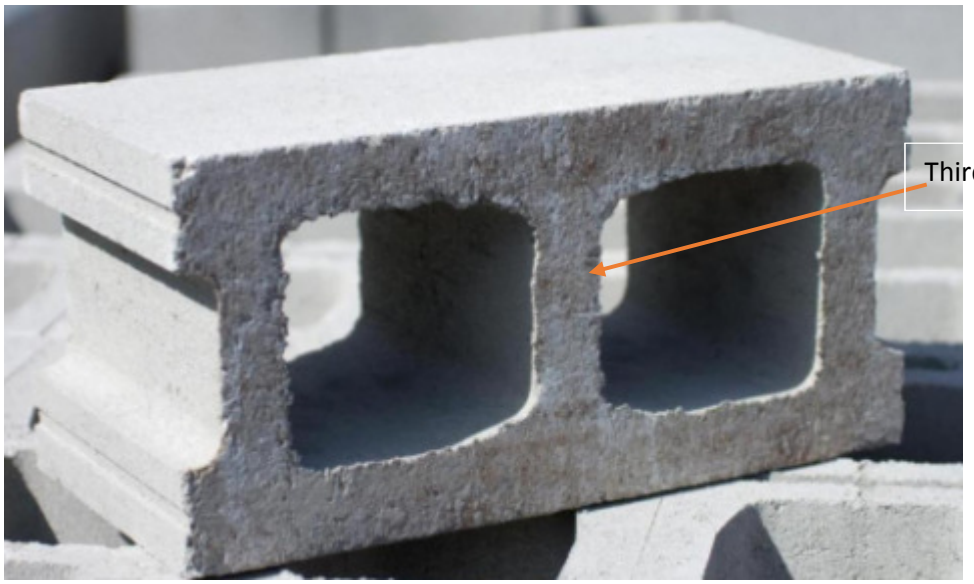

Figure 6.3. This figure represents what was meant by "the third wall" in concrete block.

4) The beams can be analyzed and tested based on scale. To see if size difference would increase or decrease the flexural capacity.
5) Testing columns made of the same material, to see if this composite would be sufficient to build an entire structure.
6) The composite can be also analyzed using different types of soil and recycled plastics.
7) Investigating the fill percentage effect on the beam.

References

Brydson, J. A. (1999). *Plastics materials*. Elsevier.

Coble, S. (2003). Materials data book. *Cambridge University Engineering Department, Cambridge, UK*.

Dodziuk, H. (2016). Applications of 3D printing in healthcare. *Kardiochirurgia i torakochirurgia polska= Polish journal of cardio-thoracic surgery*, *13*(3), 283.

"*Failure mechanisms in timber structures: Film project for educational purposes*". (n.d.). Retrieved February 10, 2018, from https://www.hb.bgu.tum.de/projekte/failure-mechanisms/

Gretsch, K. F., Lather, H. D., Peddada, K. V., Deeken, C. R., Wall, L. B., & Goldfarb, C. A. (2016). Development of novel 3D-printed robotic prosthetic for transradial amputees. *Prosthetics and orthotics international*, *40*(3), 400-403.

Gross, B. C., Erkal, J. L., Lockwood, S. Y., Chen, C., & Spence, D. M. (2014). Evaluation of 3D printing and its potential impact on biotechnology and the chemical sciences. *Analytical Chemistry*, 86(7), 3240-3253. DOI: 10.1021/ac403397r

Gutierrez, C. R. R. (2016). *Improving the engineering properties of PLA for 3D printing and beyond*. The University of Texas at El Paso.

Harper, C. A. (2000). *Modern Plastics Handbook: Handbook*. McGraw-Hill Professional.

Hejazi, S. M., Sheikhzadeh, M., Abtahi, S. M., & Zadhoush, A. (2012). A simple review of soil reinforcement by using natural and synthetic fibers. *Construction and building materials*, *30*, 100-116. https://doi.org/10.1016/j.conbuildmat.2011.11.045 (09/20/2017).

Kading, B., & Straub, J. (2015). Utilizing in-situ resources and 3D printing structures for a manned Mars mission. *Acta Astronautica*, *107*, 317-326. https://doi.org/10.1016/j.actaastro.2014.11.036 (09/20/2017)

Kopeliovich, D., "Flexural tests of ceramics." *Knowledge source on materials engineering*, <http://www.substech.com/dokuwiki/doku.php?id=flexural_strength_tests_of_ceramics> (Nov. 1, 2017)

Lee, D. H. (2014). *Deformation Behavior of Honeycomb Foams in Compression* (Doctoral dissertation, The Graduate School, Stony Brook University: Stony Brook, NY.).

Lin, J. H., Hsieh, C. T., Hu, J. J., Chen, Y. S., Chen, W. C., & Lou, C. W. (2012). Effect of heat-treated process on tensile property of PLA plied-yarn. In *Applied Mechanics and Materials*, 184, 963-966. Trans Tech Publications.

Make It From (2015) Polylactic Acid (PLA, Polylactide), from: http://www.makeitfrom.com/materialproperties/PolylacticAcidPLA-Polylactide/(Accessed: July 2015).

Make It From (2015) Acrylonitrile Butadiene Styrene (ABS), from: http://www.makeitfrom.com/materialproperties/AcrylonitrileButadieneStyrene-ABS/(Accessed: July 2015).

Panda, B., Tan, M. J., Gibson, I., & Chua, C. K. (2016). *The Disruptive Evolution Of 3D Printing*.

Panda, B., Paul, S. C., & Tan, M. J. (2017). Anisotropic mechanical performance of 3D printed fiber reinforced sustainable construction material. *Materials Letters*, *209*, 146-149. http://dx.doi.org/10.1016/j.matlet.2017.07.123

Quora (2017). *What is Strain-Stress Curve*. Retrieved January 10, 2018, from https://www.quora.com/What-is-strain-Stress-Curve

Randolph, A. F. *SPI plastics engineering handbook: of the Society of the Plastics Industry, Inc*. Reinhold.

Semuels, A. (2015). *The Resurrection of America's Slums*. Retrieved March 05, 2018, from https://www.theatlantic.com/business/archive/2015/08/more-americans-are-living-in-slums/400832/

Shing, B., & Mehrabi, A. B. (2002). *Behaviour and analysis of masonry-infilled frames*. Retrieved March 11, 2018, from https://onlinelibrary.wiley.com/doi/epdf/10.1002/pse.122

Wang, S. (2016). Additive Manufacturing Processes For Fabricating A Mini Robot-Computational Models And Experimental Results.

Vaezi, M., & Chua, C. K. (2011). Effects of layer thickness and binder saturation level parameters on 3D printing process. *The International Journal of Advanced Manufacturing Technology*, *53*(1-4), 275-284. DOI: 10.1007/s00170-010-2821-1

Ventola, C. L. (2014). Medical applications for 3D printing: current and projected uses. *Pharmacy and Therapeutics*, *39*(10), 704.

Yao, X., Luan, C., Zhang, D., Lan, L., & Fu, J. (2017). Evaluation of carbon fiber-embedded 3D printed structures for strengthening and structural-health monitoring. *Materials & Design*, *114*, 424-432. http://dx.doi.org/10.1016/j.matdes.2016.10.078.

Zareiyan, B., & Khoshnevis, B. (2017). Interlayer adhesion and strength of structures in Contour Crafting-Effects of aggregate size, extrusion rate, and layer thickness. *Automation in Construction*, *81*, 112-121.

Zhang, H. (2016). *Characterization of tensile, creep, and fatigue properties of 3D printed Acrylonitrile Butadiene Styrene*(Doctoral dissertation).

Zhang, D., Ueda, T., & Furuuchi, H. (2012). Concrete cover separation failure of overlay-strengthened reinforced concrete beams. *Construction and Building Materials*, *26*(1), 735-745.

Appendix A: Equations

$$\sigma_f = \frac{Mc}{I}$$ Equation 3.1

$$M = \frac{PL}{4}$$ Equation 3.2

$$\sigma_f = \frac{PLd}{8I}$$ Equation 3.3

$$\sigma_f = \frac{3PL}{2bd^2}$$ Equation 3.4

$$\varepsilon_f = \frac{6Dd}{L^2}$$ Equation 3.5

$$s = \sqrt{\frac{(\sum x^2 - nX^2)}{n-1}}$$ Equation 3.6